

SpookyNet: Learning Force Fields with Electronic Degrees of Freedom and Nonlocal Effects

Oliver T. Unke,^{1, 2, a} Stefan Chmiela,¹ Michael Gastegger,^{1, 2} Kristof T. Schütt,¹ Huziel E. Sauceda,^{1, 3} and Klaus-Robert Müller^{1, 4, 5, 6, b}

¹Machine Learning Group, Technische Universität Berlin, 10587 Berlin, Germany

²DFG Cluster of Excellence “Unifying Systems in Catalysis” (UniSysCat), Technische Universität Berlin, 10623 Berlin, Germany

³BASLEARN, BASF-TU joint Lab, Technische Universität Berlin, 10587 Berlin, Germany

⁴Department of Artificial Intelligence, Korea University, Anam-dong, Seongbuk-gu, Seoul 02841, Korea

⁵Max Planck Institute for Informatics, Stuhlsatzenhausweg, 66123 Saarbrücken, Germany

⁶Google Research, Brain team, Berlin, Germany

In recent years, machine-learned force fields (ML-FFs) have gained increasing popularity in the field of computational chemistry. Provided they are trained on appropriate reference data, ML-FFs combine the accuracy of *ab initio* methods with the efficiency of conventional force fields. However, current ML-FFs typically ignore electronic degrees of freedom, such as the total charge or spin, when forming their prediction. In addition, they often assume chemical locality, which can be problematic in cases where nonlocal effects play a significant role. This work introduces SpookyNet, a deep neural network for constructing ML-FFs with explicit treatment of electronic degrees of freedom and quantum nonlocality. Its predictions are further augmented with physically-motivated corrections to improve the description of long-ranged interactions and nuclear repulsion. SpookyNet improves upon the current state-of-the-art (or achieves similar performance) on popular quantum chemistry data sets. Notably, it can leverage the learned chemical insights, e.g. by predicting unknown spin states or by properly modeling physical limits. Moreover, it is able to generalize across chemical and conformational space and thus close an important remaining gap for today’s machine learning models in quantum chemistry.

Keywords: SpookyNet, machine learning, neural network, force field, potential energy surface, nonlocal, delocalized interactions, quantum nature, spooky, electronic degrees of freedom

I. INTRODUCTION

Molecular dynamics (MD) simulations of chemical systems allow to gain insights on many intricate phenomena, such as reactions or the folding of proteins.¹ To perform MD simulations, knowledge of the forces acting on individual atoms at every time step of the simulation is required.² The most accurate way of deriving these forces is by (approximately) solving the Schrödinger equation (SE), which describes the physical laws governing chemical systems.³ Unfortunately, the computational cost of accurate *ab initio* approaches⁴ makes them impractical when many atoms are studied, or the simulation involves thousands (or even millions) of time steps. For this reason, it is common practice to use force fields (FFs) – analytical expressions for the potential energy of a chemical system, from which forces are obtained by derivation – in place of a direct solution of the SE.⁵ The remaining difficulty is to find an appropriate functional form that gives forces at the required accuracy. Recently, machine learning (ML) methods have gained increasing popularity for solving this task.^{6–10} They allow to automatically learn the relation between chemical structure and forces from *ab initio* reference data. The accuracy of such ML-FFs is only limited

by the quality of the data used to train them and their computational efficiency is comparable to conventional FFs.⁷

One of the first methods for constructing ML-FFs for high-dimensional systems was introduced by Behler and Parrinello for studying the properties of bulk silicon.¹¹ The idea is to encode the local (within a certain cutoff radius) chemical environment of each atom in a descriptor, e.g. using symmetry functions,¹² which is used as input to an artificial neural network¹³ predicting atomic energies. The total potential energy of the system is the sum of the individual contributions, and forces are obtained by derivation with respect to atom positions. While it is also possible to directly predict the total energy (or forces),^{14–16} an atomic energy decomposition makes predictions extensive and the learned model applicable to systems of different size. Many other ML-FFs follow this design principle, but rely on different descriptors^{17–19} or use other ML methods,^{20–22} such as kernel machines,²³ for the prediction. An alternative to manually designed descriptors is to use the raw atomic numbers and Cartesian coordinates as input instead. Then, suitable atomic representations can be learned from (and adapted to) the reference data automatically. This is usually achieved by “passing messages” between atoms to iteratively build increasingly sophisticated descriptors in a deep neural network architecture. After the introduction of the deep tensor neural network (DTNN)²⁴, such message-passing neural networks (MPNNs)²⁵ became highly popular and

^a oliver.unke@googlemail.com

^b klaus-robert.mueller@tu-berlin.de

the original architecture has since been refined by many related approaches.^{26–28}

However, atomic numbers and Cartesian coordinates (or descriptors derived from them) do not provide an unambiguous description of chemical systems.²⁹ They only describe the nuclear degrees of freedom, but contain no information about the electronic wave function, such as the total charge or spin. This is of no concern when all systems of interest have a *consistent* electronic state (e.g. they are all neutral singlet structures), but leads to an *ill-defined* learning problem otherwise. Further, most ML-FFs assume that atomic properties are dominated by their *local* chemical environment.⁷ While this assumption is valid in many cases, it still neglects that quantum systems are inherently nonlocal in nature, a quality which Einstein famously referred to as “*spooky actions at a distance*”.³⁰ For example, electrons can be delocalized over a chemical system and charge or spin density may instantaneously redistribute to specific atoms based on distant structural changes.^{31–35}

Therefore this work introduces SpookyNet, a deep MPNN for constructing ML-FFs, which accounts for both nuclear and electronic degrees of freedom and models quantum nonlocality explicitly. Additionally, its energy predictions are augmented with (optional) physically-motivated corrections to improve the description of long-ranged electrostatic and dispersion interactions and short-ranged repulsion between nuclei.

The text is structured as follows: Section II summarizes the contributions of the present work and discusses similarities and differences to previous methods, which is followed by a detailed description of the SpookyNet architecture in Section III. Next, applications to several quantum chemistry data sets are considered: The importance of encoding electronic degrees of freedom and modelling nonlocal effects is demonstrated by ablation studies on simple model systems in Section IV A and the completeness of atomic descriptors learned by SpookyNet is investigated in Section IV B. This is followed by an evaluation of SpookyNet’s ability to generalize across chemical and conformational space (Section IV C), describe nonlocal charge transfer and different charge states (Section IV D), and predict unknown spin states (Section IV E). Specifics of the training procedure used for fitting the parameters of SpookyNet and other implementation details are given in Section V, before the results are discussed and the text is concluded in Section VI.

II. CONTRIBUTIONS AND RELATION TO PREVIOUS WORK

SpookyNet is an MPNN and, as such, shares basic design principles with predecessors such as DTNN.^{24,26} Most MPNN architectures initialize atomic feature representations with elemental embeddings, which are then updated iteratively with some kind of update function by “passing messages” between atoms.²⁵ A notable difference to pre-

vious work is the inclusion of the ground state electronic configuration when computing embeddings, which encourages chemically meaningful representations. Early MPNNs relied on purely distance-based messages,^{24,26,28} whereas later architectures such as DimeNet³⁶ proposed to include angular information in the feature updates. However, explicitly computing angles between all neighbors of an atom scales quadratically with the number of neighbors. To achieve linear scaling, SpookyNet encodes angular information implicitly via the use of novel basis functions based on Bernstein polynomials³⁷ and spherical harmonics (see also section IV B for a more detailed discussion on encoding angular information). Spherical harmonics are also used in neural network architectures for rotationally equivariant predictions, such as tensor field networks,³⁸ Cormorant,³⁹ PaiNN,⁴⁰ or NequIP.⁴¹ However, since only scalar quantities (energies) need to be predicted for constructing ML-FFs, SpookyNet projects rotationally equivariant features to invariant representations for computational efficiency. Many methods for constructing descriptors of atomic environments use similar approaches to derive rotationally invariant quantities from spherical harmonics.^{19,42,43}

To prevent quadratically scaling evaluation costs, many MPNNs introduce a (smooth) cutoff when passing messages, such that feature updates only involve a small number of neighbors in the vicinity of each atom. This can introduce artifacts beyond the cutoff radius when strong long-ranged interactions like electrostatics are of importance.²⁸ For this reason, many ML-FFs^{44–48} include analytical long-range corrections to improve their predictions. This work follows Ref. 28, i.e. both electrostatic and dispersion corrections are used and atomic partial charges and energies are predicted with a single neural network. However, the D3 dispersion correction⁴⁹ is replaced by the newer D4 variant.⁵⁰ Further, this work introduces an analytical short-range correction based on the Ziegler-Biersack-Littmark (ZBL) stopping potential⁵¹ to improve the description of nuclear repulsion.

The biggest difference to previous work is the explicit treatment of electronic degrees of freedom and nonlocal interactions. Most ML-FFs rely on nuclear charges and atomic coordinates as their only inputs and are thus unable to distinguish chemical systems with different electronic states, but there are some exceptions. For example, the charge equilibration neural network technique (CENT)⁵² was developed to construct interatomic potentials for ionic systems. In CENT, a neural network predicts atomic electronegativities (instead of energy contributions), from which partial charges are derived via a charge equilibration scheme^{53–55} that minimizes the electrostatic energy of the system and models nonlocal charge transfer. Then, the total energy is obtained by an analytical expression involving the partial charges. Since they are constrained to conserve the total charge, different charge states of the same chemical system can be treated by a single model. The recently proposed fourth-generation Behler-Parinello neural network (4G-BPNN)⁵⁶

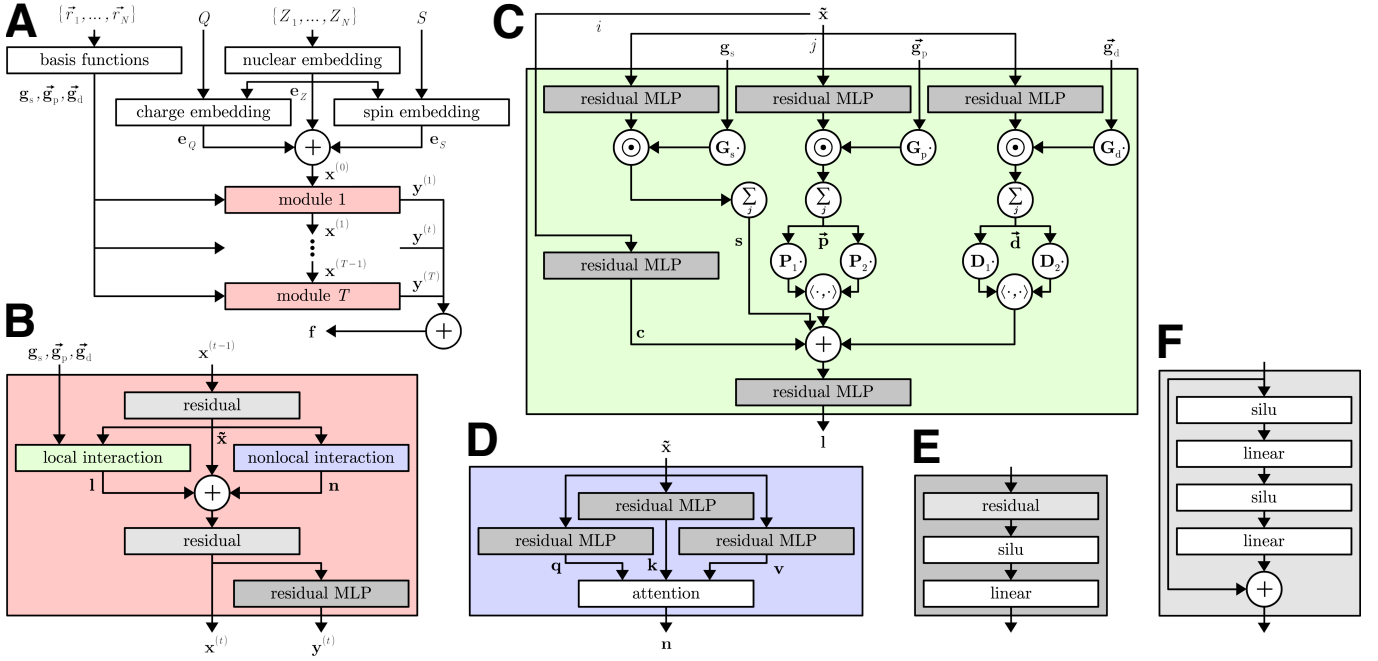


FIG. 1: Schematic depiction of the SpookyNet architecture with color-coded view of individual components. For details on the nuclear and electronic (charge/spin) embeddings and basis functions, refer to Eqs. 5, 6 and 11, respectively. **A:** Architecture overview. **B:** Interaction module, see Eq. 8. **C:** Local interaction block, see Eq. 10. **D:** Nonlocal interaction block, see Eq. 16. **E:** Residual multilayer perceptron (MLP), see Eq. 4. **F:** Pre-activation residual block, see Eq. 3.

expands on this idea using two separate neural networks: The first one predicts atomic electronegativities, from which partial charges are derived using the same method as in CENT. The second neural network predicts atomic energy contributions, receiving the partial charges as additional inputs, which contain implicit information about the total charge. Unfortunately, the charge equilibration scheme used in CENT and 4G-BPNs involves the solution of a system of linear equations, which scales cubically with the number of atoms. Further, only different total charges, but not spin states, can be distinguished with this approach.

In contrast, SpookyNet treats both, different charge *and* spin states, in a consistent manner within a single end-to-end trainable neural network, scales linearly with the number of atoms, and can learn to model arbitrary nonlocal interactions instead of being restricted to nonlocal charge transfer.

III. NEURAL NETWORK ARCHITECTURE

This section describes basic neural network building blocks and gives details on how they are combined to form the components of the SpookyNet architecture (see Fig. 1 for a schematic depiction). A summary of the notation used throughout this section and a brief overview over the prediction process can be found below.

Notation Scalar values are denoted by either lowercase a or uppercase A symbols. Vectors in abstract feature spaces are indicated by bold lowercase symbols \mathbf{v} to distinguish them from vectors with directional information (in physical space), which are written with an accented arrow \vec{v} . The notation $\tilde{\mathbf{v}}$ indicates a feature vector with an additional directional dimension, in contrast to matrices, which are written with bold uppercase symbols \mathbf{M} . Norms $\|\cdot\|$ and scalar products $\langle \cdot, \cdot \rangle$ are always computed across directional dimensions and Hadamard (element-wise) multiplication \odot implies scalar multiplication for entries with directional information. Subscript indices i are used to indicate that a quantity is affiliated with atom i , but are omitted whenever a distinction between different atoms is not necessary for clarity.

Overview SpookyNet takes sets of atomic numbers $\{Z_1, \dots, Z_N \mid Z_i \in \mathbb{N}\}$ and Cartesian coordinates $\{\vec{r}_1, \dots, \vec{r}_N \mid \vec{r}_i \in \mathbb{R}^3\}$, which describe the element types and positions of N atoms, as input. Information about the electronic wave function, which is necessary for an unambiguous description of a chemical system, is provided via two additional inputs: The total charge $Q \in \mathbb{Z}$ encodes the number of electrons (given by $Q + \sum_i Z_i$), whereas the total angular momentum is encoded as the number of unpaired electrons $S \in \mathbb{N}_0$. For example, a singlet state is indicated by $S = 0$, a doublet state by $S = 1$, and so on. SpookyNet then transforms

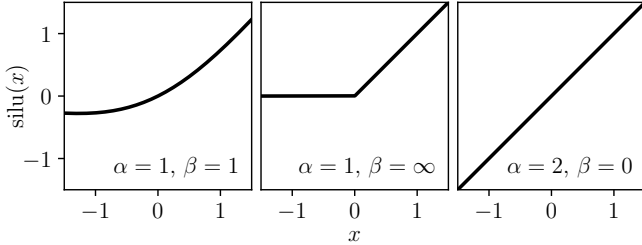


FIG. 2: Generalized SiLU activation (Eq. 2). For $\alpha = 1, \beta = \infty$, $\text{silu}(x)$ is equivalent to $\max(x, 0)$ (also known as ReLU activation), whereas for $\alpha = 2, \beta = 0$, the identity function is obtained.

these inputs to atomic descriptors $\mathbf{f} \in \mathbb{R}^F$, which contain both local information about the chemical environment of each atom and nonlocal contributions from the electronic structure. The transformation is constructed such that all \mathbf{f}_i are permutationally equivariant with respect to relabeling the atom indices i and invariant with respect to rotations and translations of the atom positions. Finally, atomic energy contributions E_i are predicted from \mathbf{f}_i via linear regression and the total potential energy E_{pot} is obtained as a sum over E_i (plus optional empirical corrections). Energy-conserving forces \vec{F}_i acting on atom i are derived from E_{pot} by automatic differentiation⁵⁷ with respect to \vec{r}_i , i.e. $\vec{F}_i = -\partial E_{\text{pot}}/\partial \vec{r}_i$.

1. Basic neural network building blocks

Linear layers Linear layers take input features $\mathbf{x} \in \mathbb{R}^{n_{\text{in}}}$ and transform them according to

$$\text{linear}(\mathbf{x}) = \mathbf{W}\mathbf{x} + \mathbf{b}, \quad (1)$$

where $\mathbf{W} \in \mathbb{R}^{n_{\text{out}} \times n_{\text{in}}}$ and $\mathbf{b} \in \mathbb{R}^{n_{\text{out}}}$ are learnable weights and biases, and n_{in} and n_{out} are the dimensions of the input and output feature space, respectively. In this work, $n_{\text{in}} = n_{\text{out}}$ unless otherwise specified.

Activation function Since Eq. 1 can only describe linear transformations, an activation function is required to learn nonlinear mappings between feature spaces. Here, a generalized SiLU (Sigmoid Linear Unit) activation function^{58,59} (also known as “swish”⁶⁰) given by

$$\text{silu}(x) = \frac{\alpha x}{1 + e^{-\beta x}} \quad (2)$$

is used. Depending on the values of α and β , Eq. 2 smoothly interpolates between a linear function and the popular ReLU (Rectified Linear Unit) activation⁶¹ (see Fig. 2). Instead of choosing arbitrary fixed values, α and β are learnable parameters in this work. Whenever the notation $\text{silu}(\mathbf{x})$ is used, Eq. 2 is applied to the vector \mathbf{x} entry-wise and separate

α and β parameters are used for each entry. Note that a smooth activation function is necessary for predicting potential energies, because the presence of kinks would introduce discontinuities in the atomic forces.

Residual blocks A combination of just two linear layers with (most) nonlinear activation functions is sufficient to approximate arbitrary functional relations between inputs and outputs, provided that a sufficiently large feature space is used in the *hidden* layer (intermediate layer between inputs and outputs).^{62,63} However, *deep* neural networks with many hidden layers stacked on top of each other often perform better in practice and were shown to be more parameter-efficient for approximating some functional relations.^{64–67} In theory, increasing the number of layers should never decrease the performance of a neural network, since in principle, superfluous layers could always learn the identity mapping. In practice, however, deeper neural networks become increasingly difficult to train due to the vanishing gradients problem,⁶⁸ which often degrades performance when too many layers are used. To combat this issue, it is common practice to introduce “shortcuts” into the architecture that skip one or several layers,⁶⁹ creating a *residual block*.⁷⁰ By inverting the order of linear layers and activation functions, it is even possible to train neural networks with several hundreds of layers.⁷¹ These “pre-activation” residual blocks transform input features \mathbf{x} according to

$$\text{residual}(\mathbf{x}) = \mathbf{x} + \text{linear}_2(\text{silu}_2(\text{linear}_1(\text{silu}_1(\mathbf{x})))) . \quad (3)$$

Residual multilayer perceptron Small feedforward neural networks consisting of a single residual block, followed by an activation and a linear output layer, are used throughout the SpookyNet architecture. For conciseness, such residual multilayer perceptrons (MLPs) are written as

$$\text{resmlp}(\mathbf{x}) = \text{linear}(\text{silu}(\text{residual}(\mathbf{x}))) . \quad (4)$$

2. SpookyNet components

Nuclear embedding The nuclear embedding is used to map atomic numbers $Z \in \mathbb{N}$ to vectors $\mathbf{e}_Z \in \mathbb{R}^F$ given by

$$\mathbf{e}_Z = \mathbf{M}\mathbf{d}_Z + \tilde{\mathbf{e}}_Z . \quad (5)$$

Here, $\mathbf{M} \in \mathbb{R}^{F \times 20}$ is a parameter matrix that projects constant element descriptors $\mathbf{d}_Z \in \mathbb{R}^{20}$ to an F -dimensional feature space and $\tilde{\mathbf{e}}_Z \in \mathbb{R}^F$ are element-specific bias parameters. The descriptors \mathbf{d}_Z encode information about the ground state electronic configuration of each element (see Table I for details). Note that the term $\tilde{\mathbf{e}}_Z$ by itself allows to learn arbitrary embeddings for different elements, but including $\mathbf{M}\mathbf{d}_Z$ provides an inductive bias to learn representations that capture similarities between different elements, i.e. contain alchemical knowledge.

element	Z	1s	2s	2p	3s	3p	4s	3d	4p	5s	4d	5p	6s	4f	5d	6p	vs	vp	vd	vf
H	$\mathbf{d}'_1 = [\begin{array}{cccccccccccccccccc} 1 & 1 & 0 & 0 & 0 & 0 & 0 & 0 & 0 & 0 & 0 & 0 & 0 & 0 & 0 & 0 & 0 & 1 & 0 & 0 & 0 \end{array}]^T$																			
C	$\mathbf{d}'_6 = [\begin{array}{cccccccccccccccccc} 6 & 2 & 2 & 2 & 0 & 0 & 0 & 0 & 0 & 0 & 0 & 0 & 0 & 0 & 0 & 0 & 0 & 2 & 2 & 0 & 0 \end{array}]^T$																			
N	$\mathbf{d}'_7 = [\begin{array}{cccccccccccccccccc} 7 & 2 & 2 & 3 & 0 & 0 & 0 & 0 & 0 & 0 & 0 & 0 & 0 & 0 & 0 & 0 & 0 & 2 & 3 & 0 & 0 \end{array}]^T$																			
O	$\mathbf{d}'_8 = [\begin{array}{cccccccccccccccccc} 8 & 2 & 2 & 4 & 0 & 0 & 0 & 0 & 0 & 0 & 0 & 0 & 0 & 0 & 0 & 0 & 0 & 2 & 4 & 0 & 0 \end{array}]^T$																			
P	$\mathbf{d}'_{15} = [\begin{array}{cccccccccccccccccc} 15 & 2 & 2 & 6 & 2 & 3 & 0 & 0 & 0 & 0 & 0 & 0 & 0 & 0 & 0 & 0 & 0 & 2 & 3 & 0 & 0 \end{array}]^T$																			
S	$\mathbf{d}'_{16} = [\begin{array}{cccccccccccccccccc} 16 & 2 & 2 & 6 & 2 & 4 & 0 & 0 & 0 & 0 & 0 & 0 & 0 & 0 & 0 & 0 & 0 & 2 & 4 & 0 & 0 \end{array}]^T$																			
Fe	$\mathbf{d}'_{26} = [\begin{array}{cccccccccccccccccc} 26 & 2 & 2 & 6 & 2 & 6 & 2 & 6 & 0 & 0 & 0 & 0 & 0 & 0 & 0 & 0 & 0 & 2 & 0 & 6 & 0 \end{array}]^T$																			
I	$\mathbf{d}'_{53} = [\begin{array}{cccccccccccccccccc} 53 & 2 & 2 & 6 & 2 & 6 & 2 & 10 & 6 & 2 & 10 & 5 & 0 & 0 & 0 & 0 & 0 & 2 & 5 & 10 & 0 \end{array}]^T$																			
Au	$\mathbf{d}'_{79} = [\begin{array}{cccccccccccccccccc} 79 & 2 & 2 & 6 & 2 & 6 & 2 & 10 & 6 & 2 & 10 & 6 & 1 & 14 & 10 & 0 & 1 & 0 & 10 & 14 \end{array}]^T$																			
Rn	$\mathbf{d}'_{86} = [\begin{array}{cccccccccccccccccc} 86 & 2 & 2 & 6 & 2 & 6 & 2 & 10 & 6 & 2 & 10 & 6 & 2 & 14 & 10 & 6 & 2 & 6 & 10 & 14 \end{array}]^T$																			

TABLE I: Examples of element descriptors. Here, unscaled descriptors \mathbf{d}'_Z are shown. The entries encode information about the ground state electron configuration (e.g. $1s^2 2s^2 2p^2$ for C), the total number of electrons/nuclear charge (e.g. $Z = 7$ for N), and the number of electrons in the valence shells (e.g. $vs^2 vp^4$ for O). The descriptors used in Eq. 5 are given by $\mathbf{d}_Z = \mathbf{d}'_Z \oslash \mathbf{d}'_{86}$, where \oslash denotes Hadamard (element-wise) division (such that all entries of \mathbf{d}_Z lie between 0 and 1, which is desirable for numerical reasons). In this work, it is assumed that $Z_{\max} = 86$ covers most practical applications, but descriptors for heavier elements could be derived analogously (and the scaling procedure adapted accordingly if necessary).

Electronic embedding Electronic embeddings are used to map the total charge $Q \in \mathbb{Z}$ and number of unpaired electrons $S \in \mathbb{N}_0$ to vectors $\mathbf{e}_Q, \mathbf{e}_S \in \mathbb{R}^F$, which delocalize this information over all atoms via a mechanism similar to attention.⁷² The mapping is given by

$$\mathbf{q} = \text{linear}(\mathbf{e}_Z), \mathbf{k} = \begin{cases} \tilde{\mathbf{k}}_+ & \Psi \geq 0 \\ \tilde{\mathbf{k}}_- & \Psi < 0 \end{cases}, \mathbf{v} = \begin{cases} \tilde{\mathbf{v}}_+ & \Psi \geq 0 \\ \tilde{\mathbf{v}}_- & \Psi < 0 \end{cases},$$

$$a_i = \frac{\Psi \ln \left(1 + \exp \left(\mathbf{q}_i^T \mathbf{k} / \sqrt{F} \right) \right)}{\sum_{j=1}^N \ln \left(1 + \exp \left(\mathbf{q}_j^T \mathbf{k} / \sqrt{F} \right) \right)}, \mathbf{e}_\Psi = \text{resmlp}(a\mathbf{v}), \quad (6)$$

where $\tilde{\mathbf{k}}, \tilde{\mathbf{v}} \in \mathbb{R}^F$ are parameters and $\Psi = Q$ for charge embeddings, or $\Psi = S$ for spin embeddings (independent parameters are used for each type of electronic embedding). Separate parameters indicated by subscripts $+/ -$ are used for positive and negative total charge inputs Q (since S is always positive or zero, only the $+$ -parameters are used for spin embeddings). Here, all bias terms in the resmlp transformation (Eq. 4) are removed, such that when $a\mathbf{v} = \mathbf{0}$, the electronic embedding $\mathbf{e}_\Psi = \mathbf{0}$ as well. Note that $\sum_i a_i = \Psi$, i.e. the electronic information is distributed across atoms with weights proportional to the scaled dot product $\mathbf{q}_i^T \mathbf{k} / \sqrt{F}$.

Interaction module The nuclear and electronic embeddings are used to define initial atomic representations

$$\mathbf{x}^{(0)} = \mathbf{e}_Z + \mathbf{e}_Q + \mathbf{e}_S, \quad (7)$$

which are refined iteratively by a chain of T interaction modules according to

$$\begin{aligned} \tilde{\mathbf{x}} &= \text{residual}_1(\mathbf{x}^{(t-1)}), \\ \mathbf{x}^{(t)} &= \text{residual}_2(\tilde{\mathbf{x}} + \mathbf{l} + \mathbf{n}), \\ \mathbf{y}^{(t)} &= \text{resmlp}(\mathbf{x}^{(t)}). \end{aligned} \quad (8)$$

Here, $\tilde{\mathbf{x}} \in \mathbb{R}^F$ are temporary atomic features and $\mathbf{l}, \mathbf{n} \in \mathbb{R}^F$ represent interactions with other atoms. They are computed by local (Eq. 10) and nonlocal (Eq. 16) interaction blocks, respectively, which are described further below. Each module t produces two outputs $\mathbf{x}^{(t)}, \mathbf{y}^{(t)} \in \mathbb{R}^F$, where $\mathbf{x}^{(t)}$ is the input to the next module in the chain and all $\mathbf{y}^{(t)}$ outputs are accumulated to the final atomic descriptors

$$\mathbf{f} = \sum_{t=1}^T \mathbf{y}^{(t)}. \quad (9)$$

Local interaction block The features \mathbf{l} in Eq. 8 represent a local interaction of atoms within a cutoff radius $r_{\text{cut}} \in \mathbb{R}$ and introduce information about the atom positions $\vec{r} \in \mathbb{R}^3$. They are computed from the temporary features $\tilde{\mathbf{x}}$ (see Eq. 8) according to

$$\begin{aligned} \mathbf{c} &= \text{resmlp}_c(\tilde{\mathbf{x}}), \\ \mathbf{s}_i &= \sum_{j \in \mathcal{N}(i)} \text{resmlp}_s(\tilde{\mathbf{x}}_j) \odot (\mathbf{G}_s \mathbf{g}_s(\vec{r}_{ij})), \\ \vec{\mathbf{p}}_i &= \sum_{j \in \mathcal{N}(i)} \text{resmlp}_p(\tilde{\mathbf{x}}_j) \odot (\mathbf{G}_p \vec{\mathbf{g}}_p(\vec{r}_{ij})), \\ \vec{\mathbf{d}}_i &= \sum_{j \in \mathcal{N}(i)} \text{resmlp}_d(\tilde{\mathbf{x}}_j) \odot (\mathbf{G}_d \vec{\mathbf{g}}_d(\vec{r}_{ij})), \\ \mathbf{l} &= \text{resmlp}_l \left(\mathbf{c} + \mathbf{s} + \langle \mathbf{P}_1 \vec{\mathbf{p}}, \mathbf{P}_2 \vec{\mathbf{p}} \rangle + \langle \mathbf{D}_1 \vec{\mathbf{d}}, \mathbf{D}_2 \vec{\mathbf{d}} \rangle \right), \end{aligned} \quad (10)$$

where, $\mathcal{N}(i)$ is the set of all indices $j \neq i$ for which $\|\vec{r}_{ij}\| < r_{\text{cut}}$ (with $\vec{r}_{ij} = \vec{r}_j - \vec{r}_i$). The parameter matrices $\mathbf{G}_s, \mathbf{G}_p, \mathbf{G}_d \in \mathbb{R}^{F \times K}$ are used to construct feature-wise interaction functions as linear combinations of basis functions $\mathbf{g}_s \in \mathbb{R}^K$, $\vec{\mathbf{g}}_p \in \mathbb{R}^{K \times 3}$, and $\vec{\mathbf{g}}_d \in \mathbb{R}^{K \times 5}$ (see Eq. 11), which have the same rotational symmetries as

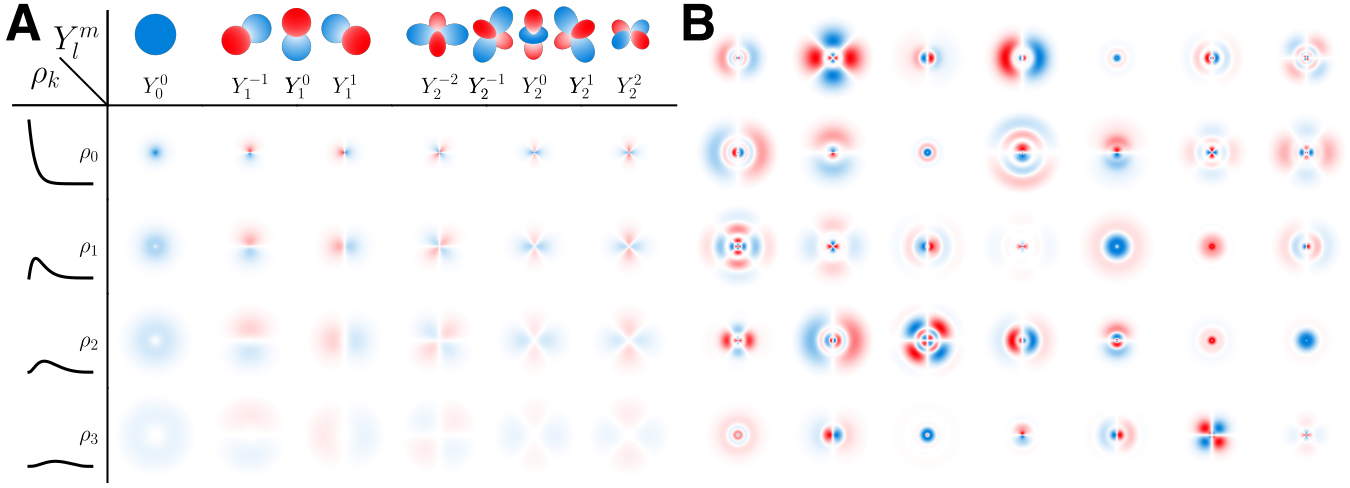


FIG. 3: **A:** Two-dimensional cuts of basis functions with $K = 4$ (see Eq. 11) with different radial and angular components ρ_k (Eq. 12) and Y_l^m (Eq. 15). **B:** Visualization of randomly chosen learned interaction functions for SpookyNet trained on the QM7-X⁷³ dataset ($K = 16$).

s-, p-, and d-orbitals (see Fig. 3). The features $\mathbf{s} \in \mathbb{R}^F$, $\vec{\mathbf{p}} \in \mathbb{R}^{F \times 3}$, and $\vec{\mathbf{d}} \in \mathbb{R}^{F \times 5}$ encode the arrangement of neighboring atoms within the cutoff radius and $\mathbf{c} \in \mathbb{R}^F$ describes the central atom in each neighborhood. Here, \mathbf{s} stores purely radial information, whereas $\vec{\mathbf{p}}$ and $\vec{\mathbf{d}}$ allow to resolve angular information in a computationally efficient manner (see also Section IV B). The parameter matrices $\mathbf{P}_1, \mathbf{P}_2, \mathbf{D}_1, \mathbf{D}_2 \in \mathbb{R}^{F \times F}$ are used to compute two independent linear projections for each of the rotationally equivariant features $\vec{\mathbf{p}}$ and $\vec{\mathbf{d}}$, from which rotationally invariant features are obtained via a scalar product $\langle \cdot, \cdot \rangle$. Contrary to simply taking the norm over the directional dimension, this method of scalarization allows non-trivial mixing between different feature channels.

The basis functions are given by

$$\begin{aligned} \mathbf{g}_s(\vec{r}) &= \begin{bmatrix} 0g_0^0 \\ \vdots \\ K-1g_0^0 \end{bmatrix}, \\ \vec{\mathbf{g}}_p(\vec{r}) &= \begin{bmatrix} 0g_1^{-1} & 0g_1^0 & 0g_1^1 \\ \vdots & \vdots & \vdots \\ K-1g_1^{-1} & K-1g_1^0 & K-1g_1^1 \end{bmatrix}, \\ \vec{\mathbf{g}}_d(\vec{r}) &= \begin{bmatrix} 0g_2^{-2} & 0g_2^{-1} & 0g_2^0 & 0g_2^1 & 0g_2^2 \\ \vdots & \vdots & \vdots & \vdots & \vdots \\ K-1g_2^{-2} & K-1g_2^{-1} & K-1g_2^0 & K-1g_2^1 & K-1g_2^2 \end{bmatrix}, \\ k\mathbf{g}_l^m &= \rho_k(\|\vec{r}\|) \cdot Y_l^m(\vec{r}), \end{aligned} \quad (11)$$

where the radial component ρ_k is

$$\rho_k(r) = b_{k,K-1}(\exp(-\gamma r)) \cdot f_{\text{cut}}(r) \quad (12)$$

and

$$b_{k,K-1}(x) = \binom{K-1}{k} x^k (1-x)^{K-1-k} \quad (13)$$

are Bernstein polynomials ($k = 0, \dots, K-1$). The hyper-parameter K determines the total number of radial components (and the degree of the Bernstein polynomials). For $K \rightarrow \infty$, linear combinations of $b_{k,K-1}(x)$ can approximate any continuous function on the interval $[0, 1]$ uniformly.³⁷ An exponential function $\exp(-\gamma r)$ maps distances r from $[0, \infty)$ to the interval $(0, 1]$, where $\gamma \in \mathbb{R}_{>0}$ is a radial decay parameter shared across all basis functions (for computational efficiency). A desirable side effect of this mapping is that the rate at which learned interaction functions can vary decreases with increasing r , which introduces a chemically meaningful inductive bias (electronic wave functions also decay exponentially with increasing distance from a nucleus).^{28,74} The cutoff function

$$f_{\text{cut}}(r) = \begin{cases} \exp\left(-\frac{r^2}{(r_{\text{cut}} - r)(r_{\text{cut}} + r)}\right) & r < r_{\text{cut}} \\ 0 & r \geq r_{\text{cut}} \end{cases} \quad (14)$$

ensures that basis functions smoothly decay to zero for $r \geq r_{\text{cut}}$, so that no discontinuities are introduced when atoms enter or leave the cutoff radius. The angular component

$Y_l^m(\vec{r})$ in Eq. 11 is given by

$$\begin{aligned} Y_l^m(\vec{r}) &= \begin{cases} \sqrt{2} \cdot \Pi_l^{|m|}(z) \cdot A_{|m|}(x, y) & m < 0 \\ \Pi_l^0(z) & m = 0 \\ \sqrt{2} \cdot \Pi_l^m(z) \cdot B_m(x, y) & m > 0 \end{cases}, \\ A_m(x, y) &= \sum_{p=0}^m \binom{m}{p} x^p y^{m-p} \sin\left(\frac{\pi}{2}(m-p)\right), \\ B_m(x, y) &= \sum_{p=0}^m \binom{m}{p} x^p y^{m-p} \cos\left(\frac{\pi}{2}(m-p)\right), \\ \Pi_l^m(z) &= \sqrt{\frac{(l-m)!}{(l+m)!}} \sum_{p=0}^{\lfloor(l-m)/2\rfloor} c_{plm} r^{2p-l} z^{l-2p-m}, \\ c_{plm} &= \frac{(-1)^p}{2^l} \binom{l}{p} \binom{2l-2p}{l} \frac{(l-2p)!}{(l-2p-m)!}, \end{aligned} \quad (15)$$

where $\vec{r} = [x \ y \ z]^\top$ and $r = \|\vec{r}\|$. Note that the Y_l^m in Eq. 15 omit the normalization constant $\sqrt{(4\pi)/(2l+1)}$, but are otherwise identical to the standard (real) spherical harmonics.

Nonlocal interaction block Although locality is a valid assumption for many chemical systems,⁷ electrons may also be delocalized across multiple distant atoms. Starting from the temporary features $\tilde{\mathbf{x}}$ (see Eq. 8), such nonlocal interactions are modeled via *self-attention*⁷² as

$$\begin{aligned} \mathbf{q}_i &= \text{resmlp}_q(\tilde{\mathbf{x}}_i), & \mathbf{Q} &= [\mathbf{q}_1 \cdots \mathbf{q}_N]^\top, \\ \mathbf{k}_i &= \text{resmlp}_k(\tilde{\mathbf{x}}_i), & \mathbf{K} &= [\mathbf{k}_1 \cdots \mathbf{k}_N]^\top, \\ \mathbf{v}_i &= \text{resmlp}_v(\tilde{\mathbf{x}}_i), & \mathbf{V} &= [\mathbf{v}_1 \cdots \mathbf{v}_N]^\top, \\ \mathbf{N} &= \text{attention}(\mathbf{Q}, \mathbf{K}, \mathbf{V}), & \mathbf{N} &= [\mathbf{n}_1 \cdots \mathbf{n}_N]^\top, \end{aligned} \quad (16)$$

where the features \mathbf{n} in Eq. 8 are the (transposed) rows of the matrix $\mathbf{N} \in \mathbb{R}^{N \times F}$. The idea of attention is inspired by retrieval systems,⁷⁵ where a *query* is mapped against *keys* to retrieve the best-matched corresponding *values* from a database. Standard attention is computed as

$$\begin{aligned} \mathbf{A} &= \exp\left(\mathbf{Q}\mathbf{K}^\top/\sqrt{F}\right), & \mathbf{D} &= \text{diag}(\mathbf{A}\mathbf{1}_N), \\ \text{attention}(\mathbf{Q}, \mathbf{K}, \mathbf{V}) &= \mathbf{D}^{-1}\mathbf{AV}, \end{aligned} \quad (17)$$

where $\mathbf{Q}, \mathbf{K}, \mathbf{V} \in \mathbb{R}^{N \times F}$ are queries, keys, and values, $\mathbf{1}_N$ is the all-ones vector of length N , and $\text{diag}(\cdot)$ is a diagonal matrix with the input vector as the diagonal. Unfortunately, computing attention with Eq. 17 has a time and space complexity of $\mathcal{O}(N^2F)$ and $\mathcal{O}(N^2 + NF)$,⁷⁶ respectively, because the attention matrix $\mathbf{A} \in \mathbb{R}^{N \times N}$ has to be stored explicitly. Since quadratic scaling with the number of atoms N is problematic for large chemical systems, the FAVOR+ (Fast Attention Via positive Orthogonal

Random features) approximation⁷⁶ is used instead:

$$\begin{aligned} \widehat{\mathbf{Q}} &= [\phi(\mathbf{q}_1) \cdots \phi(\mathbf{q}_N)]^\top, & \widehat{\mathbf{K}} &= [\phi(\mathbf{k}_1) \cdots \phi(\mathbf{k}_N)]^\top, \\ \widehat{\mathbf{D}} &= \text{diag}\left(\widehat{\mathbf{Q}}\left(\widehat{\mathbf{K}}^\top \mathbf{1}_N\right)\right), \\ \text{attention}(\mathbf{Q}, \mathbf{K}, \mathbf{V}) &= \widehat{\mathbf{D}}^{-1}(\widehat{\mathbf{Q}}(\widehat{\mathbf{K}}^\top \mathbf{V})). \end{aligned} \quad (18)$$

Here $\phi : \mathbb{R}^F \mapsto \mathbb{R}_{>0}^f$ is a mapping designed to approximate the softmax kernel via f random features, see Ref. 76 for details (here, $f = F$ for simplicity). The time and space complexities for computing attention with Eq. 18 are $\mathcal{O}(NFF)$ and $\mathcal{O}(NF + Nf + Ff)$,⁷⁶ i.e. both scale linearly with the number of atoms N . To make the evaluation of SpookyNet deterministic, the random features of the mapping ϕ are drawn only once at initialization and kept fixed afterwards (instead of redrawing them for each evaluation). Note that attention allows information to be communicated between all atoms in the system, regardless of their distance.

Potential energy prediction Once all interaction modules are evaluated, atomic energy contributions E_i are predicted from the atomic descriptors \mathbf{f}_i via linear regression:

$$E_i = \mathbf{w}_E^\top \mathbf{f}_i + \tilde{E}_{Z_i}. \quad (19)$$

Here, $\mathbf{w}_E \in \mathbb{R}^F$ are the regression weights and $\tilde{E}_Z \in \mathbb{R}$ are element-dependent energy biases. The total potential energy is given by

$$E_{\text{pot}} = \sum_{i=1}^N E_i + E_{\text{rep}} + E_{\text{ele}} + E_{\text{vdw}}, \quad (20)$$

where E_{rep} , E_{ele} , and E_{vdw} are (optional) empirical corrections, which augment the energy prediction with physical knowledge.

Nuclear repulsion is modeled by the term E_{rep} , which is based on the Ziegler-Biersack-Littmark stopping potential⁵¹ and given by

$$\begin{aligned} E_{\text{rep}} &= k_e \sum_i \sum_{j>i \in \mathcal{N}(i)} \frac{Z_i Z_j}{r_{ij}} f_{\text{cut}}(r_{ij}) \cdot \\ &\quad \left(\sum_{k=1}^4 c_k e^{-a_k r_{ij} (Z_i^p + Z_j^p)/d} \right). \end{aligned} \quad (21)$$

Here, k_e is the Coulomb constant and a_k , c_k , p , and d are parameters (see Eqs. 10 and 14 for the definitions of $\mathcal{N}(i)$ and f_{cut}).

Long-range electrostatic interactions are modeled as

$$E_{\text{ele}} = k_e \sum_i \sum_{j>i} q_i q_j \left(\frac{f_{\text{switch}}(r_{ij})}{\sqrt{r_{ij}^2 + 1}} + \frac{1 - f_{\text{switch}}(r_{ij})}{r} \right), \quad (22)$$

where q_i are atomic partial charges predicted from the atomic features \mathbf{f}_i according to

$$q_i = \mathbf{w}_q^T \mathbf{f}_i + \tilde{q}_{Z_i} + \frac{1}{N} \left[Q - \sum_{j=1}^N (\mathbf{w}_q^T \mathbf{f}_j + \tilde{q}_{Z_j}) \right]. \quad (23)$$

Here, $\mathbf{w}_q \in \mathbb{R}^F$ and $\tilde{q}_Z \in \mathbb{R}$ are regression weights and element-dependent biases, respectively. The second half of the equation ensures that $\sum_i q_i = Q$, i.e. the total charge is conserved. Note that Eq. 22 smoothly interpolates between the correct r^{-1} behavior of Coulomb's law at large distances ($r > r_{\text{off}}$) and a damped ($r_{ij}^2 + 1)^{-1/2}$ dependence at short distances ($r < r_{\text{on}}$) via a smooth switching function f_{switch} given by

$$\sigma(x) = \begin{cases} \exp(-\frac{1}{x}) & x > 0 \\ 0 & x \leq 0 \end{cases},$$

$$f_{\text{switch}}(r) = \frac{\sigma\left(1 - \frac{r-r_{\text{on}}}{r_{\text{off}}-r_{\text{on}}}\right)}{\sigma\left(1 - \frac{r-r_{\text{on}}}{r_{\text{off}}-r_{\text{on}}}\right) + \sigma\left(\frac{r-r_{\text{on}}}{r_{\text{off}}-r_{\text{on}}}\right)}. \quad (24)$$

For simplicity, $r_{\text{on}} = \frac{1}{4}r_{\text{cut}}$ and $r_{\text{off}} = \frac{3}{4}r_{\text{cut}}$, i.e. the switching interval is automatically adjusted depending on the chosen cutoff radius r_{cut} (see Eq. 14). It should be noted that it is also possible to construct dipole moments $\vec{\mu}$ from the partial charges according to

$$\vec{\mu} = \sum_{i=1}^N q_i \vec{r}_i, \quad (25)$$

which can be useful for calculating infrared spectra from MD simulations and for fitting q_i to *ab initio* reference data without imposing arbitrary charge decomposition schemes⁷⁷ (see Section V for details).

Long-range dispersion interactions are modeled via the term E_{vdw} . Analytical van der Waals corrections are an active area of research and many different methods, for example the Tkatchenko-Scheffler correction,⁷⁸ or many body dispersion,⁷⁹ have been proposed.⁸⁰ In this work, the two-body term of the D4 dispersion correction⁵⁰ is used for its simplicity and computational efficiency:

$$E_{\text{vdw}} = - \sum_i \sum_{j>i} \sum_{n=6,8} s_n \frac{C_{(n)}^{ij}}{r_{ij}^n} f_{\text{damp}}^{(n)}(r_{ij}). \quad (26)$$

Here s_n are scaling parameters, $f_{\text{damp}}^{(n)}$ is a damping function, and $C_{(n)}^{ij}$ are pairwise dispersion coefficients. They are obtained by interpolating between tabulated reference values based on a (geometry-dependent) fractional coordination number and an atomic partial charge q_i . In the standard D4 scheme, the partial charges are obtained via a charge equilibration scheme,⁵⁰ in this work, however, the q_i from Eq. 23 are used instead. Note that the D4 method was developed mainly to correct for the lack of dispersion in density functionals,⁵⁰ so typically, some of

its parameters are adapted to the functional the correction is applied to (optimal values for each functional are determined by fitting to high-quality electronic reference data). In this work, all D4 parameters that vary between different functionals are treated as learnable parameters when SpookyNet is trained, i.e. they are automatically adapted to the reference data. Since Eq. 23 (instead of charge equilibration) is used to determine the partial charges, an additional learnable parameter s_q is introduced to scale the tabulated reference charges used to determine dispersion coefficients $C_{(n)}^{ij}$. For further details on the implementation of the D4 method, the reader is referred to Ref. 50.

IV. RESULTS

A. Ablation studies

Most current quantum chemistry benchmarks only contain neutral singlet structures dominated by local effects, which makes it difficult to show the benefits of including electronic embeddings (Eq. 6) or nonlocal interactions (Eq. 16). To motivate these additions, three toy tasks are introduced and it is demonstrated how the performance of SpookyNet degrades when crucial components of the architecture are disabled (all model variants are trained from scratch). The results of these ablation studies are summarized in Fig. 4A–C.

In the first task (A), a single model must learn to predict different conformations of both Ag_3^+ and Ag_3^- . This problem cannot be solved without the ability to encode information about the total molecular charge, because models need to be able to distinguish between similar arrangements of atoms for both structures. Consequently, when the charge embedding \mathbf{e}_Q is removed from Eq. 7, the quality of predictions decreases drastically. For example, when SpookyNet is used for geometry optimizations, an ablated model predicts wrong global minima, whereas a regular model leads to structures virtually indistinguishable from the reference (see Fig. 4A). This is also reflected in the corresponding energy predictions: While a regular model predicts potential energies with errors of only a few meV, the errors of an ablated model are more than three orders of magnitude larger. Note that even without a charge encoding, the ablated model is able to predict different minima for Ag_3^+ and Ag_3^- . This is because its potential energy predictions are still augmented with explicit point charge electrostatics (see Eq. 22) and the atomic partial charges q_i (see Eq. 23) are constrained such that $\sum_i q_i = Q$, i.e. the total molecular charge is conserved. However, such implicit information is insufficient to distinguish both charge states adequately.

The second task (B) is similar, but $\text{Ag}_3^+/\text{Ag}_3^-$ is replaced with singlet/triplet CH_2 . Without incorporating spin states in the molecular representation, this problem is equally unsolvable. In this case, contrary to the previous example, the necessary information is not even included

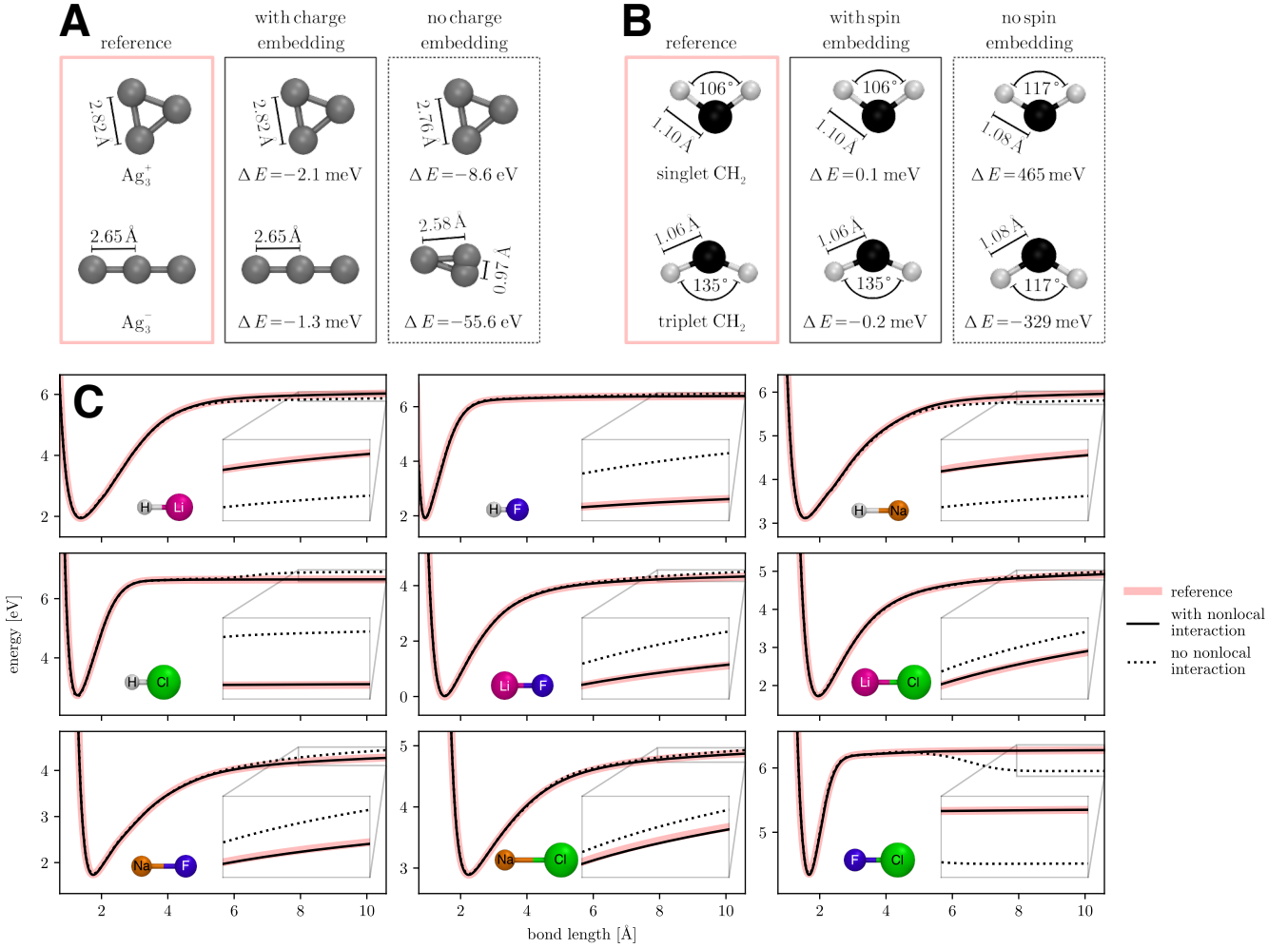


FIG. 4: **A:** Optimized geometries and prediction errors (ΔE) for the minimum energy of Ag_3^+ and Ag_3^- obtained from SpookyNet with and without a charge embedding. **B:** Optimized geometries and prediction errors (ΔE) for the minimum energy of singlet and triplet CH_2 obtained from SpookyNet with and without a spin embedding. **C:** Dissociation curves of different diatomic molecules predicted by SpookyNet with and without nonlocal interactions (both variants include the physical correction terms in Eq. 20).

implicitly when the spin embedding \mathbf{e}_S is removed. Consequently, an ablated model cannot distinguish between both systems of interest and must find a compromise between the (from its perspective) contradictory labels. This is especially apparent when looking at optimized geometries (see Fig. 4B): While a regular model agrees well with the reference and predicts potential energies with errors below 1 meV, an ablated model optimizes both spin states to the same structure (which agrees with neither the singlet nor triplet reference) and its errors are larger by more than three orders of magnitude.

The last task (C) is to learn the dissociation curves of nine (neutral singlet) diatomic molecules made up of H, Li, F, Na, and Cl atoms. Once the bonding partners are separated by more than the chosen cutoff radius r_{cut} , models that rely only on local information will always predict the same energy contributions for atoms of the same

element (by construction). However, since electrons are free to distribute unevenly across atoms, even when they are separated (e.g. due to differences in their electronegativity), energy contributions should always depend on the presence of other atoms in the structure. Consequently, it is difficult for models without nonlocal interactions to predict the correct asymptotic behavior for all systems simultaneously. As such, when the nonlocal features \mathbf{n} are removed from interaction modules (Eq. 8), SpookyNet predicts a (smooth) “step” for large interatomic separations, even when a large cutoff of $r_{\text{cut}} = 18 a_0$ ($\approx 9.52519 \text{ \AA}$) is used (see Fig. 4C). While this does not lead to any discontinuities in the potential energy surface due to the way the cutoff function is designed (see Eq. 14), such artifacts would still be problematic when simulating reactions. Simply increasing the cutoff is no adequate solution to this problem, since it just shifts the artifacts to larger dis-

tances. Similarly, the inclusion of long-range corrections is also insufficient to avoid problems in the asymptotic tails (all analytical corrections for predicting the potential energy are enabled for both models). It should be noted that the problems described above for models without nonlocal interactions can only be observed when a single model is used to fit all diatomic systems at the same time. When fitted on just one or two systems, models can partially compensate for nonlocal interactions with the bias term \tilde{E}_Z in Eq. 19. With sufficiently many systems however, there are insufficient degrees of freedom in the bias parameters to “cheat” in this way.

B. Completeness of atomic descriptors in SpookyNet

Many ML algorithms for constructing potential energy surfaces make use of some sort of descriptor to represent atoms in their chemical environment. As long as this description is *complete*, any atom-centered property (including atomic decompositions of extensive properties such as energy) can be predicted from the descriptors.⁸² In this context, *completeness* means that structures which are not convertible into each other (by translations, rotations, or permutations of equivalent atoms) map to different descriptors.

A simple descriptor for the environment of an atom i at position \vec{r}_i consists of the set of distances $r_{ij} = \|\vec{r}_{ij}\|$ (with $\vec{r}_{ij} = \vec{r}_j - \vec{r}_i$) to neighboring atoms j , and the set of angles

$$\alpha_{ijk} = \arccos \left(\frac{\langle \vec{r}_{ij}, \vec{r}_{ik} \rangle}{\|\vec{r}_{ij}\| \|\vec{r}_{ik}\|} \right) \quad (27)$$

between all possible combinations of neighboring atoms j and k . For environments consisting of multiple different species, separate sets of distances (and angles) are necessary for each element (or combination of elements). However, for simplicity, it is assumed here that all atoms are identical. A disadvantage of using angles in the descriptor is that their computation scales $\mathcal{O}(n^2)$ with the number of neighbors n , because all combinations must be considered. An alternative to encode angular information, which scales $\mathcal{O}(n)$, is to replace the set of angles with invariants of the form

$$a_{i,l} = \sum_{m=-l}^l \left(\sum_{j=1}^n Y_l^m(\vec{r}_{ij}) \right)^2 \quad (28)$$

derived from the angular power spectrum, where Y_l^m are the spherical harmonics (see Eq. 15). In the following, $a_{i,l}$ for $l = 0, 1, 2, 3, 4$ are called s, p, d, f, and g invariants because of their relation to the symmetries of atomic orbitals. The disadvantage here is that when using a finite number ($l = 0, \dots, L$) of power spectrum invariants as angular descriptor, some environments with different sets of angles may lead to the same descriptor. For

example, square planar and tetrahedral environments have the same s and p invariants ($L = 1$), so it is necessary to include at least d invariants ($L = 2$) in the descriptor to differentiate them (see Fig. 5B).

There is a widespread belief in the literature that sets of distances and angles are sufficient for a *complete* description of atomic environments.^{83,84} However, it was recently demonstrated that this is not the case, and even including the set of dihedrals

$$\delta_{ijkl} = \arccos \left(\frac{\langle \vec{r}_{ij} \times \vec{r}_{ik}, \vec{r}_{ik} \times \vec{r}_{il} \rangle}{\|\vec{r}_{ij} \times \vec{r}_{ik}\| \|\vec{r}_{ik} \times \vec{r}_{il}\|} \right) \quad (29)$$

between triplets of neighboring atoms does not lead to a *complete* description in general.⁸¹ In this context, it is interesting to investigate the *completeness* of the atomic descriptors \mathbf{f} (see Eq. 9) learned by SpookyNet and compare its ability to distinguish different structures to other popular approaches. For this purpose, five pairs of distinct atomic environments (shown in Fig. 5A–E), with geometries that are particularly difficult to separate, are considered. Then, different models are trained to predict scalar labels of 1 (for one of the environments) and −1 (for the other environment) from the descriptors of the central atoms (blue) in each pair. It can be observed that models either learn to predict the labels with virtually zero error (up to numerical precision), i.e. the environments can be distinguished, or a value of 0 is predicted for both central atoms, i.e. their environments are mapped to the same descriptor and a compromise between the contradictory labels has to be found. The results are summarized in Table II.

Most models based on hand-crafted descriptors can only distinguish environments when their sets of distances and angles (and in some cases dihedrals) differs. Message-passing neural networks (MPNNs) on the other hand can learn to distinguish all environments shown in Fig. 5, provided that at least $T \geq 2$ message-passing steps are used. The amount of information that can be resolved with a single message-passing step ($T = 1$) is often related to the power spectrum invariants (see Eq. 28) and different MPNNs mainly differ in the maximum order L which they can resolve in a single update (with the exception of DimeNet,³⁶ which uses angles directly but scales $\mathcal{O}(n^2)$ with the number of neighbors n). SpookyNet uses an update with a maximum order of $L = 2$, which is sufficient to differentiate most common chemical environments (as long as they are distinguishable by distances and angles). It would be possible to introduce higher order interactions with the symmetry of f-, or even g-orbitals into the update step (see Eq. 10), so that additional environments (e.g. Fig. 5D) become distinguishable with a single update, but this increases the computational cost and is found to give little benefit (in terms of additional accuracy for predictions) in practice.

Pozdnyakov *et al.* propose a different *completeness* test

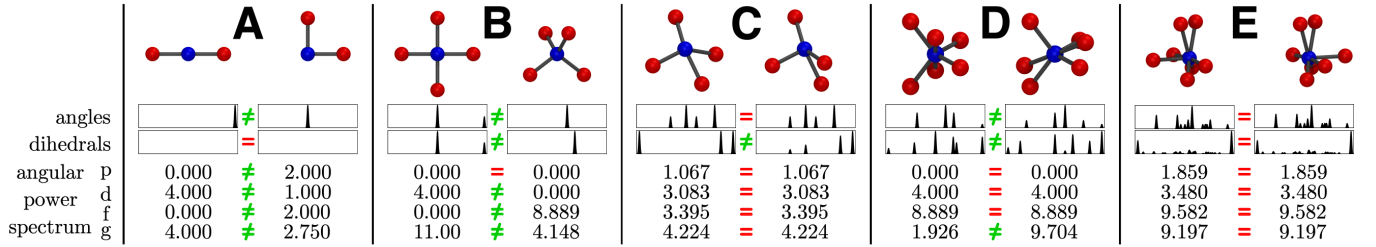


FIG. 5: Pairs of distinct atomic environments where all neighboring atoms (red) have the same distance from the central atom (blue). The distributions of angles (Eq. 27) and dihedrals (Eq. 29) are visualized and values of the angular power spectrum invariants (Eq. 28) for different angular momenta $l = 1, \dots, 4$ (p, d, f, g) are given for each structure (the s invariant simply counts the number of neighbors and is therefore omitted). Since all distances to neighboring atoms are identical, descriptors need to be able to at least resolve angular information to distinguish the structures (**A**). However, for some structures, the power spectrum invariants may be degenerate for small values of l (**B** and **D**). Some structures even have identical angular distributions, in which case the power spectrum invariants are equal for all $l = 0, \dots, \infty$ and information about dihedrals is necessary to distinguish the environments (**C**). Note that some environments cannot even be distinguished when information about dihedrals is included (**E**).⁸¹

model	scaling	A	B	C	D	E
hand-crafted descriptors						
BPNN ¹¹	$\mathcal{O}(n^2)$	✓	✓	✗	✓	✗
FCHL19 ²²	$\mathcal{O}(n^2)$	✓	✓	✗	✓	✗
FCHL18 ⁸⁵	$\mathcal{O}(n^3)$ *	✓	✓	✓**	✓	✗
learned descriptors						
SchNet ²⁶	$\mathcal{O}(n)$	(✓)	(✓)	(✓)	(✓)	(✓)
PhysNet ²⁸	$\mathcal{O}(n)$	(✓)	(✓)	(✓)	(✓)	(✓)
DimeNet ³⁶	$\mathcal{O}(n^2)$	✓	✓	(✓)	✓	(✓)
NequIP ⁴¹	$\mathcal{O}(n)$	✓	(✓)	(✓)	(✓)	(✓)
PaiNN ⁴⁰	$\mathcal{O}(n)$	✓	(✓)	(✓)	(✓)	(✓)
SpookyNet	$\mathcal{O}(n)$	✓	✓	(✓)	(✓)	(✓)

* when dihedrals are included

** only distinguishable with dihedrals

TABLE II: Ability of models to differentiate the atomic environments shown in Fig. 5 (✓: distinguishable, ✗: indistinguishable) and the scaling of their computational cost with respect to the number of neighbors n . Message-passing neural networks with learned descriptors can distinguish all environments when there are $T \geq 2$ message-passing steps. However, when only a single step is used ($T = 1$), the environments marked with (✓) become indistinguishable.

based on a data set of $\sim 7.7\text{M}$ CH_4 structures⁸⁶ that were generated by randomly placing H atoms in a 3 \AA sphere around the C atom (see Ref. 81 for details). Due to the strongly distorted geometries, potential energies in this data set vary by $\sim 1400 \text{ kcal mol}^{-1}$ and forces by $\sim 10700 \text{ kcal mol}^{-1} \text{ \AA}^{-1}$. Further, this way of sampling will lead to many structures with (nearly) degenerate sets of angles (see Fig. 5C) and is thus particularly challenging to learn. For this task, it is to be expected that models relying on *incomplete* descriptors improve at a slower rate (and eventually cease to improve at all) when increasing the number of training data.⁸¹ The performance of

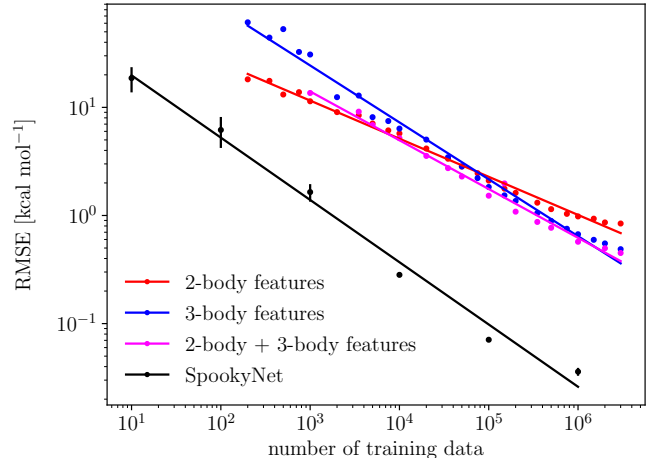


FIG. 6: Energy learning curves for the random CH_4 dataset⁸⁶ suggested in Ref. 81. SpookyNet (black) is compared to feedforward neural networks trained on 2-body and/or 3-body features (red, blue, magenta), see Ref. 81 for details.

SpookyNet on this data set for different training set sizes is summarized in Table III. With only 10 training points ($\sim 0.00013\%$ of the data), SpookyNet reaches prediction errors that correspond to a relative absolute error of just $\sim 1\%$ (with respect to the energy range covered in the data set). Chemical accuracy (absolute errors $< 1 \text{ kcal mol}^{-1}$) is reached with as few as 1000 training points. The learning curve (see Fig. 6) shows that the performance of SpookyNet increases steadily when more data is used for training while being about two orders of magnitude more data-efficient than other methods.

n_{train}	energy [kcal mol ⁻¹]		forces [kcal mol ⁻¹ Å ⁻¹]	
	MAE	RMSE	MAE	RMSE
10	11.698 (2.440)	18.650 (4.889)	14.426 (3.280)	40.302 (16.473)
100	4.011 (1.688)	6.183 (1.969)	5.782 (1.436)	14.345 (4.730)
1 000	0.607 (0.030)	1.646 (0.304)	1.360 (0.039)	5.326 (2.614)
10 000	0.078 (0.002)	0.282 (0.009)	0.249 (0.007)	0.998 (0.032)
100 000	0.020 (0.001)	0.071 (0.003)	0.071 (0.001)	0.326 (0.012)
1 000 000	0.020 (0.002)	0.036 (0.003)	0.063 (0.006)	0.165 (0.015)

TABLE III: Mean absolute errors (MAEs) and root mean square errors (RMSEs) of energies and forces for the random CH₄ dataset⁸⁶ suggested in Ref. 81. Results are averaged over 16 ($n_{\text{train}} = 10$), 8 ($n_{\text{train}} = 100$), or 4 ($n_{\text{train}} \geq 1000$) random splits and the standard deviation between runs is given in brackets.

C. Generalization across chemical and conformational space

In this section, SpookyNet is applied to the MD17¹⁵ and QM7-X⁷³ data sets, which probe generalization across different aspects of chemical space.

MD17 MD17 consists of structures, energies, and forces collected from *ab initio* MD simulations of small organic molecules at the PBE+TS^{78,87} level of theory. Trajectories were calculated at a temperature of 500 K, a resolution of 0.5 fs, and contain between $\sim 10^5$ – 10^6 conformations. Potential energies vary between ~ 20 – 48 kcal mol⁻¹ and forces between ~ 266 – 570 kcal mol⁻¹ Å⁻¹, depending on the molecule. This data set probes the ability of ML models to generalize to unseen conformations of a single molecule from a relatively small training set. Prediction errors for several models published in the literature are summarized in Table IV and compared to SpookyNet, which improves upon or closely matches the previous state-of-the-art for all molecules.

QM7-X QM7-X was generated starting from ~ 7 k molecular graphs with up to seven non-hydrogen atoms (C, N, O, S, Cl) drawn from the GDB13 database.⁸⁸ Structural and constitutional (stereo)isomers were sampled and optimized for each graph, leading to ~ 42 k equilibrium structures. For each of these, an additional 100 non-equilibrium structures were generated by displacing atoms along linear combinations of normal modes corresponding to a temperature of 1500 K, which leads to ~ 4.2 M structures in total. For each of these, QM7-X contains data for 42 physicochemical properties (see Ref. 73 for a complete list). For constructing ML-FFs, however, the properties E_{tot} and F_{tot} , which correspond to energies and forces computed at the PBE0+MBD^{79,89} level of theory, are the most relevant. Within non-equilibrium conformations sampled around the same minimum structure, the energy varies between ~ 3 – 20 eV and forces between ~ 10 – 103 eV Å⁻¹, i.e. the range of energies and forces is almost one order of magnitude larger than in MD17.

Because of the variety of molecules contained in the QM7-X data set, it is ideal to check the ability

of a model to generalize across both chemical and conformational space when large amounts of training data are available. Such a setting is interesting for constructing general ML-FFs that are applicable to multiple different molecules. Here, two variants are considered: In the more challenging task (unknown molecules/unknown conformations), a total of 10100 entries corresponding to all structures sampled for 25 out of the original ~ 7 k molecular graphs are reserved as test set and the model is trained on the remainder of the data. In this setting, all structures in the test set correspond to unknown molecules, i.e. the model has to learn general principles of chemistry to perform well. As comparison, an easier task (known molecules/unknown conformations) is constructed by randomly choosing 10100 entries as test set, so it is very likely that the training set contains at least some structures for all molecules contained in QM7-X. In the easy setting, the model only has to generalize to unknown conformations (similar to MD17). Interestingly, the performance of SpookyNet is only marginally worse when predicting unknown molecules (see Table V), suggesting that it successfully generalizes across chemical space. Note, that in addition to energies and forces, SpookyNet uses dipole moments (property D) to fit partial charges (see Section V), for which errors are also reported.

D. Nonlocal charge transfer

To demonstrate the ability of SpookyNet to model nonlocal charge transfer and different charge states, four test systems⁹⁰ introduced in Ref. 56 are considered. The first system (C₁₀H₂/C₁₀H₃⁺) is a linear organic molecule consisting of a chain of ten sp-hybridized C atoms terminated by H. When one end of the chain is protonated, the electronic structure along the whole chain is modified. The second system (Ag₃^{+/−}) is a small metal cluster of Ag atoms carrying either a positive or negative charge. Depending on the charge state, the Ag atoms either prefer a triangular or linear configuration (see also Section IV A, where the same system is used). As a third system (Na_{8/9}Cl₈⁺), positively charged cluster ions

		sGDML ¹⁶	SchNet ²⁶	PhysNet ²⁸	FCHL19 ²²	PaiNN ⁴⁰	SpookyNet
Aspirin	<i>energy</i>	0.19	0.37	0.230	0.182	0.159	0.151 (0.008)
	<i>forces</i>	0.68	1.35	0.605	0.478	0.371	0.258 (0.034)
Ethanol	<i>energy</i>	0.07	0.08	0.059	0.054	0.063	0.052 (0.001)
	<i>forces</i>	0.33	0.39	0.160	0.136	0.230	0.094 (0.011)
Malondialdehyde	<i>energy</i>	0.10	0.13	0.094	0.081	0.091	0.079 (0.002)
	<i>forces</i>	0.41	0.66	0.319	0.245	0.319	0.167 (0.015)
Naphthalene	<i>energy</i>	0.12	0.16	0.142	0.117	0.117	0.116 (0.001)
	<i>forces</i>	0.11	0.58	0.310	0.151	0.083	0.089 (0.018)
Salicylic acid	<i>energy</i>	0.12	0.20	0.126	0.114	0.114	0.114 (0.004)
	<i>forces</i>	0.28	0.85	0.337	0.221	0.209	0.180 (0.040)
Toluene	<i>energy</i>	0.10	0.12	0.100	0.098	0.097	0.094 (0.001)
	<i>forces</i>	0.14	0.57	0.191	0.203	0.102	0.087 (0.014)
Uracil	<i>energy</i>	0.11	0.14	0.108	0.104	0.104	0.105 (0.001)
	<i>forces</i>	0.24	0.56	0.218	0.105	0.140	0.119 (0.021)

TABLE IV: Mean absolute errors for energy (kcal mol⁻¹) and force (kcal mol⁻¹ Å⁻¹) predictions for the MD17 benchmark. Results for SpookyNet are averaged over ten random splits, the standard deviation between runs is given in brackets. All models are trained on 1000 data points (separate models are used for each molecule), best results in bold.

		energy	forces	dipole
known molecules/	MAE	18.513	39.863	39.380
unknown conformations	RMSE	29.885	65.810	58.874
unknown molecules/	MAE	20.490	46.567	41.766
unknown conformations	RMSE	28.740	74.700	61.062

TABLE V: Mean absolute errors (MAEs) and root mean square errors (RMSEs) of energies (meV), forces (meV Å⁻¹) and dipole moments (mD) for the QM7-X⁷³ dataset. The ID numbers (`idmol` field in the QM7-X file format) of the 25 molecules used as a test set in the “unknown molecules/unknown conformations” setting are: 1771, 1805, 1824, 2020, 2085, 2117, 3019, 3108, 3190, 3217, 3257, 3329, 3531, 4010, 4181, 4319, 4713, 5174, 5370, 5580, 5891, 6315, 6583, 6809, 7020.

of either eight or nine Na atoms and eight Cl atoms are considered. When the ninth Na atom is removed, the positive charge is redistributed throughout the remaining cluster. The last system (Au₂-MgO) is a diatomic Au cluster deposited on a MgO(001) surface (periodic boundary conditions are applied). Either a pure MgO lattice is used, or three Mg atoms (far from the surface) are replaced by Al. The Au₂ cluster either prefers a configuration where it stands upright on the surface on top of an O atom (pure MgO lattice), or where it lies parallel to the surface above two Mg atoms (Al-doped lattice). In other words, the presence of Al dopant atoms nonlocally modifies the electronic structure at the surface in such a way that a different Au₂ configuration becomes more stable.

Table VI summarizes the performance of SpookyNet

on the four data sets and compares them to the results reported in Ref. 56. Since Hirshfeld charges⁹¹ for all data sets are available in addition to energies and forces, prediction errors for charges are also included. SpookyNet significantly improves upon the values reported for 4G-BPNNs,⁵⁶ increasing the prediction errors by up to two orders of magnitude. For the Au₂-MgO system, which uses periodic boundary conditions, Ewald summation⁹² is used to evaluate the long-ranged empirical correction terms in Eq. 20.

E. Predicting unknown spin states

To test the ability of SpookyNet to predict energies for unknown spin states, the QMspin database⁹³ is considered. It consists of ~13k carbene structures with at most nine non-hydrogen atoms (C, N, O, F), which were optimized either in a singlet or triplet state. For each of these, both singlet and triplet energies computed at the MRCISD+Q-F12/cc-pVDZ-F12 level of theory are reported, giving a total of ~26k energy-structure pairs in the database (see Ref. 94 for more details). The energies span a range of ~11679 eV, however, the difference between singlet and triplet energy for the same structure is at most ~5.4 eV. For the lack of other models evaluated on this data set, SpookyNet is compared to an ablated variant without spin embedding, which serves as a base line. The ablated model only reaches a mean absolute prediction error (MAE) of 444.6 meV. As expected, the performance of SpookyNet is drastically improved when the spin embedding is included, allowing it to generalize to unknown spin states and reach an MAE of 68.0 meV. Both models were trained on 20k points, used 1k samples as validation set, and were tested

		2G-BPNN	3G-BPNN	4G-BPNN	SpookyNet
C₁₀H₂/C₁₀H₃⁺	<i>energy</i>	1.619	2.045	1.194	0.364
	<i>forces</i>	129.5	231.0	78.00	5.802
	<i>charges</i>	—	20.08	6.577	0.117
Na_{8/9}Cl₈⁺	<i>energy</i>	1.692	2.042	0.481	0.135
	<i>forces</i>	57.39	76.67	32.78	1.052
	<i>charges</i>	—	20.80	15.83	0.111
Ag₃⁺⁻	<i>energy</i>	352.0	320.2	1.323	0.220
	<i>forces</i>	1803	1913	31.69	26.64
	<i>charges</i>	—	26.48	9.976	0.459
Au₂-MgO	<i>energy</i>	2.287	—	0.219	0.107
	<i>forces</i>	153.1	—	66.0	5.337
	<i>charges</i>	—	—	5.698	1.013

TABLE VI: Root mean square errors (RMSEs) of energies (meV/atom), forces (meV Å⁻¹) and charges (me) for the datasets introduced in Ref. 56. The values for 2G-, 3G-, and 4G-BPNNs are taken from Ref. 56. Best results in bold. For details on the number of training/validation data used for each data set, refer to Ref. 56 (all models use the same settings).

on the remaining data.

V. METHODS

Initialization and hyperparameters All SpookyNet models in this work use $T = 6$ interaction modules, $F = 128$ features, and a cutoff radius $r_{\text{cut}} = 10 a_0$ (≈ 5.29177 Å), unless otherwise specified. Weights are initialized as random (semi-)orthogonal matrices with entries scaled according to the Glorot initialization scheme.⁶⁸ An exception are the weights of the second linear layer in residual blocks (linear₂ in Eq. 3) and the matrix \mathbf{M} used in nuclear embeddings (Eq. 5), which are initialized with zeros. All bias terms and the $\tilde{\mathbf{k}}$ and $\tilde{\mathbf{v}}$ parameters in the electronic embedding (Eq. 6) are also initialized with zeros. The parameters for the activation function (Eq. 2) start as $\alpha = 1.0$ and $\beta = 1.702$, following the recommendations given in Ref. 58. The radial decay parameter γ used in Eq. 12 is initialized to $\frac{1}{2} a_0^{-1}$ and constrained to positive values. The parameters of the empirical nuclear repulsion term (Eq. 21) start from the literature values of the ZBL potential⁵¹ and are constrained to positive values (coefficients c_k are further constrained such that $\sum c_k = 1$ to guarantee the correct asymptotic behavior for short distances). Parameters of the dispersion correction (Eq. 26) start from the values recommended for Hartree-Fock calculations⁵⁰ and the charge scaling parameter s_q is initialized to 1 (and constrained to remain positive).

Training procedure The parameters of SpookyNet are trained by minimizing a loss function with mini-batch gradient descent using the AMSGrad optimizer⁹⁵ with the recommended default momentum hyperparameters and an initial learning rate of 10^{-3} . During training, an exponential moving average of all model parameters is

kept using a smoothing factor of 0.999. Every 1k training steps, a model using the averaged parameters is evaluated on the validation set and the learning rate is decayed by a factor of 0.5 whenever the validation loss does not decrease for 25 consecutive evaluations. Training is stopped when the learning rate drops below 10^{-5} and the model that performed best on the validation set is selected. The loss function is given by

$$\mathcal{L} = \alpha_E \mathcal{L}_E + \alpha_F \mathcal{L}_F + \alpha_\mu \mathcal{L}_\mu, \quad (30)$$

where \mathcal{L}_E , \mathcal{L}_F , and \mathcal{L}_μ are separate loss terms for energies, forces and dipole moments and α_E , α_F , and α_μ corresponding weighting hyperparameters that determine the relative influence of each term to the total loss. The energy loss is given by

$$\mathcal{L}_E = \sqrt{\frac{1}{B} \sum_{b=1}^B \left(E_{\text{pot},b} - E_{\text{pot},b}^{\text{ref}} \right)^2}, \quad (31)$$

where B is the number of structures in the mini-batch, $E_{\text{pot},b}$ the predicted potential energy (Eq. 20) for structure b and $E_{\text{pot},b}^{\text{ref}}$ the corresponding reference energy. The batch size B is chosen depending on the available training data: When training sets contain 1k structures or less, $B = 1$, for 10k structures or less, $B = 10$, and for more than 10k structures, $B = 100$. The force loss is given by

$$\mathcal{L}_F = \sqrt{\frac{1}{B} \sum_{b=1}^B \left(\frac{1}{N_b} \sum_{i=1}^{N_b} \left\| -\frac{\partial E_{\text{pot},b}}{\partial \vec{r}_{i,b}} - \vec{F}_{i,b}^{\text{ref}} \right\|^2 \right)}, \quad (32)$$

where N_b is the number of atoms in structure b and $\vec{F}_{i,b}^{\text{ref}}$ the reference force acting on atom i in structure b . The dipole loss

$$\mathcal{L}_\mu = \sqrt{\frac{1}{B} \sum_{b=1}^B \left\| \left(\sum_{i=1}^{N_b} q_{i,b} \vec{r}_{i,b} \right) - \vec{\mu}_b^{\text{ref}} \right\|^2} \quad (33)$$

allows to learn partial charges (Eq. 23) from reference dipole moments $\vec{\mu}_b^{\text{ref}}$, which are, in contrast to arbitrary charge decompositions, true quantum mechanical observables.⁷⁷ Note that for charged molecules, the dipole moment is dependent on the origin of the coordinate system, so consistent conventions must be used. For some data sets or applications, however, reference partial charges $q_{i,b}^{\text{ref}}$ obtained from a charge decomposition scheme, e.g. Hirshfeld charges,⁹¹ might be preferred (or the only data available). In this case, the term $\alpha_\mu \mathcal{L}_\mu$ in Eq. 30 is replaced by $\alpha_q \mathcal{L}_q$ with

$$\mathcal{L}_q = \sqrt{\frac{1}{B} \sum_{b=1}^B \left(\frac{1}{N_b} \sum_{i=1}^{N_b} (q_{i,b} - q_{i,b}^{\text{ref}})^2 \right)}. \quad (34)$$

For simplicity, the relative loss weights are set to $\alpha_E = \alpha_F = \alpha_{\mu/q} = 1$ in this work, with exception of the MD17 data set, for which $\alpha_F = 100$ is used following previous work.²⁸ Note that the relative weight of loss terms also depends on the chosen unit system (atomic units are used here). For data sets that lack the reference data necessary for computing any of the loss terms given Eqs. 31–34, the corresponding weight is set to zero. In addition, whenever no reference data (neither dipole moments nor reference partial charges) are available to fit partial charges, both E_{ele} and E_{vdw} are omitted when predicting the potential energy E_{pot} (see Eq. 20).

Data sets used in ablation studies For the ablation studies in Section IV A, energies, forces, and dipoles for three new data sets were computed at the semi-empirical GFN2-xTB level of theory.⁹⁶ Both the $\text{Ag}_3^+/\text{Ag}_3^-$ (see Fig. 4A) and the singlet/triplet CH_2 (see Fig. 4B) data sets were computed by sampling 550 structures around the minima of both electronic states with normal mode sampling¹⁷ at 1000 K. Then, each sampled structure was re-computed in the other electronic state (e.g. all structures sampled for Ag_3^+ were re-computed with a negative charge), leading to a total of 2200 structures for each data set (models were trained on a subset of 1000 randomly sampled structures).

The data set for Fig. 4C was computed by performing bond scans for all nine shown diatomic molecules using 1k points spaced evenly between 1.5–20 a_0 , leading to a total of 9k structures. Models were trained on all data with an increased cutoff $r_{\text{cut}} = 18 a_0$ to demonstrate that a model without nonlocal interactions is unable to fit the data, even when it is allowed to overfit and use a large cutoff.

Software used for comparing the completeness of atomic descriptors Table II in Section IV B compares the ability of several published methods to distinguish the atomic environments shown in Fig. 5A–E. For evaluating PhysNet²⁸ and DimeNet,³⁶ the reference implementations available from <https://github.com/MMunibas/PhysNet> and <https://github.com/klicperajo/dimenet> are used. PaiNN⁴⁰ and NequIP⁴¹ are evaluated using in-house

implementations. For BPNN and SchNet, the implementations available in SchNetPack⁹⁷ are used. The FCHL18/19^{22,85} models are evaluated using the QML package.⁹⁸ Note that for constructing Table II, models were trained on multiple randomly rotated versions of the environments shown in Fig. 5A–E. This is done to prevent models picking up on differences due to floating point imprecision, which otherwise may make environments distinguishable even when their descriptors are degenerate (up to numerical noise).

VI. DISCUSSION AND CONCLUSION

In the present work, the SpookyNet neural network architecture is introduced and its performance for several quantum chemical systems is evaluated. SpookyNet models electronic degrees of freedom and nonlocal interactions using attention,^{72,76} which is shown to be crucial for modeling some chemical systems. Further, SpookyNet is augmented with physically-motivated empirical corrections and uses chemically meaningful inductive biases in its design. It matches or improves upon the previous state-of-the-art in several benchmark tasks. Further, evaluating SpookyNet scales as $\mathcal{O}(N)$ with the number of atoms N , unless empirical long-range corrections are used, which scale as $\mathcal{O}(N^2)$. However, this is a well-known problem, and several methods to achieve $\mathcal{O}(N \log N)$ scaling have been developed for evaluating long-ranged interactions in conventional force fields, which can also be applied here.^{99,100}

Future research could investigate the ability of SpookyNet to learn ML-FFs that generalize across many different elements of the periodic table or applications to large molecular systems.

DATA AND CODE AVAILABILITY

The data sets used for the ablation studies in Section IV A, the geometries of the structures shown in Fig. 5, and a reference implementation of SpookyNet using PyTorch¹⁰¹ will be made available when the manuscript is accepted. All other data sets used in this work are publicly available from Ref. 86 (completeness test in Section IV B), <http://www.sgdml.org> (MD17), Ref. 102 (QM7-X), Ref. 90 (data sets used in Section IV D), and Ref. 93 (QMspin).

ACKNOWLEDGMENTS

OTU acknowledges funding from the Swiss National Science Foundation (Grant No. P2BSP2_188147). We thank the authors of Ref. 81 for sharing raw data for reproducing the learning curves shown in Fig. 6 and the geometries displayed in Fig. 5E. KRM was supported in part by the Institute of Information & Communications

Technology Planning & Evaluation (IITP) grant funded by the Korea Government (No. 2019-0-00079, Artificial Intelligence Graduate School Program, Korea University), and was partly supported by the German Ministry for Education and Research (BMBF) under Grants 01IS14013A-E, 01GQ1115, 01GQ0850, 01IS18025A and 01IS18037A; the German Research Foundation (DFG) under Grant Math+, EXC 2046/1, Project ID 390685689. Correspondence should be addressed to OTU and KRM. We thank Alexandre Tkatchenko and Hartmut Maennel for very helpful discussions and feedback on the manuscript.

REFERENCES

- [1] A. Warshel, Molecular dynamics simulations of biological reactions, *Accounts of Chemical Research* **35**, 385 (2002).
- [2] M. Karplus and J. A. McCammon, Molecular dynamics simulations of biomolecules, *Nature Structural Biology* **9**, 646 (2002).
- [3] P. A. M. Dirac, Quantum mechanics of many-electron systems, *Proceedings of the Royal Society of London A* **123**, 714 (1929).
- [4] M. S. Gordon and M. W. Schmidt, Theory and applications of computational chemistry: The first forty years, *Dykstra, CE* , 1167 (2005).
- [5] O. T. Unke, D. Koner, S. Patra, S. Käser, and M. Meuwly, High-dimensional potential energy surfaces for molecular simulations: from empiricism to machine learning, *Machine Learning: Science and Technology* **1**, 013001 (2020).
- [6] M. Rupp, A. Tkatchenko, K.-R. Müller, and O. A. Von Lilienfeld, Fast and accurate modeling of molecular atomization energies with machine learning, *Physical Review Letters* **108**, 058301 (2012).
- [7] O. T. Unke, S. Chmiela, H. E. Sauceda, M. Gastegger, I. Poltavsky, K. T. Schütt, A. Tkatchenko, and K.-R. Müller, Machine learning force fields, *Chemical Reviews* (2021).
- [8] O. A. von Lilienfeld, K.-R. Müller, and A. Tkatchenko, Exploring chemical compound space with quantum-based machine learning, *Nature Reviews Chemistry* **4**, 347 (2020).
- [9] F. Noé, A. Tkatchenko, K.-R. Müller, and C. Clementi, Machine learning for molecular simulation, *Annual Review of Physical Chemistry* **71**, 361 (2020).
- [10] J. A. Keith, V. Vassilev-Galindo, B. Cheng, S. Chmiela, M. Gastegger, K.-R. Müller, and A. Tkatchenko, Combining machine learning and computational chemistry for predictive insights into chemical systems, *arXiv preprint arXiv:2102.06321* (2021).
- [11] J. Behler and M. Parrinello, Generalized neural-network representation of high-dimensional potential-energy surfaces, *Physical Review Letters* **98**, 146401 (2007).
- [12] J. Behler, Atom-centered symmetry functions for constructing high-dimensional neural network potentials, *The Journal of Chemical Physics* **134**, 074106 (2011).
- [13] W. S. McCulloch and W. Pitts, A logical calculus of the ideas immanent in nervous activity, *Bulletin of Mathematical Biophysics* **5**, 115 (1943).
- [14] O. T. Unke and M. Meuwly, Toolkit for the construction of reproducing kernel-based representations of data: Application to multidimensional potential energy surfaces, *Journal of Chemical Information and Modeling* **57**, 1923 (2017).
- [15] S. Chmiela, A. Tkatchenko, H. E. Sauceda, I. Poltavsky, K. T. Schütt, and K.-R. Müller, Machine learning of accurate energy-conserving molecular force fields, *Science advances* **3**, e1603015 (2017).
- [16] S. Chmiela, H. E. Sauceda, I. Poltavsky, K.-R. Müller, and A. Tkatchenko, sGMDL: Constructing accurate and data efficient molecular force fields using machine learning, *Computer Physics Communications* **240**, 38 (2019).
- [17] J. S. Smith, O. Isayev, and A. E. Roitberg, ANI-1: an extensible neural network potential with DFT accuracy at force field computational cost, *Chemical Science* **8**, 3192 (2017).
- [18] L. Zhang, J. Han, H. Wang, R. Car, and E. Weinan, Deep potential molecular dynamics: a scalable model with the accuracy of quantum mechanics, *Physical Review Letters* **120**, 143001 (2018).
- [19] O. T. Unke and M. Meuwly, A reactive, scalable, and transferable model for molecular energies from a neural network approach based on local information, *The Journal of Chemical Physics* **148**, 241708 (2018).
- [20] A. P. Bartók, M. C. Payne, R. Kondor, and G. Csányi, Gaussian approximation potentials: The accuracy of quantum mechanics, without the electrons, *Physical Review Letters* **104**, 136403 (2010).
- [21] A. P. Bartók, S. De, C. Poelking, N. Bernstein, J. R. Kermode, G. Csányi, and M. Ceriotti, Machine learning unifies the modeling of materials and molecules, *Science Advances* **3**, e1701816 (2017).
- [22] A. S. Christensen, L. A. Bratholm, F. A. Faber, and O. Anatole von Lilienfeld, Fchl revisited: Faster and more accurate quantum machine learning, *The Journal of Chemical Physics* **152**, 044107 (2020).
- [23] K.-R. Müller, S. Mika, G. Ratsch, K. Tsuda, and B. Schölkopf, An introduction to kernel-based learning algorithms, *IEEE Transactions on Neural Networks* **12**, 181 (2001).
- [24] K. T. Schütt, F. Arbabzadah, S. Chmiela, K. R. Müller, and A. Tkatchenko, Quantum-chemical insights from deep tensor neural networks, *Nature communications* **8**, 13890 (2017).
- [25] J. Gilmer, S. S. Schoenholz, P. F. Riley, O. Vinyals, and G. E. Dahl, Neural message passing for quantum chemistry, in *International Conference on Machine Learning* (2017) pp. 1263–1272.
- [26] K. T. Schütt, H. E. Sauceda, P.-J. Kindermans, A. Tkatchenko, and K.-R. Müller, SchNet – a deep learning architecture for molecules and materials, *The Journal of Chemical Physics* **148**, 241722 (2018).
- [27] N. Lubbers, J. S. Smith, and K. Barros, Hierarchical modeling of molecular energies using a deep neural network, *The Journal of Chemical Physics* **148**, 241715 (2018).
- [28] O. T. Unke and M. Meuwly, PhysNet: A neural network for predicting energies, forces, dipole moments, and partial charges, *Journal of Chemical Theory and Computation* **15**, 3678 (2019).
- [29] R. A. Friesner, *Ab initio* quantum chemistry: Methodology and applications, *Proceedings of the National Academy of Sciences* **102**, 6648 (2005).
- [30] M. Born and A. Einstein, *The Born-Einstein Letters 1916–1955* (Macmillan, 2005).

- [31] L. Noodleman, C. Peng, D. Case, and J.-M. Mouesca, Orbital interactions, electron delocalization and spin coupling in iron-sulfur clusters, *Coordination Chemistry Reviews* **144**, 199 (1995).
- [32] A. Dreuw, J. L. Weisman, and M. Head-Gordon, Long-range charge-transfer excited states in time-dependent density functional theory require non-local exchange, *The Journal of Chemical Physics* **119**, 2943 (2003).
- [33] L.-C. Duda, T. Schmitt, M. Magnuson, J. Forsberg, A. Olsson, J. Nordgren, K. Okada, and A. Kotani, Resonant inelastic X-Ray scattering at the oxygen K resonance of NiO: Nonlocal charge transfer and double-singlet excitations, *Physical Review Letters* **96**, 067402 (2006).
- [34] A. Bellec, D. Riedel, G. Dujardin, O. Boudrioua, L. Chapat, L. Stauffer, and P. Sonnet, Nonlocal activation of a bistable atom through a surface state charge-transfer process on Si(100)-(2×1):H, *Physical Review Letters* **105**, 048302 (2010).
- [35] E. V. Boström, A. Mikkelsen, C. Verdozzi, E. Perfetto, and G. Stefanucci, Charge separation in donor-C₆₀ complexes with real-time green functions: The importance of nonlocal correlations, *Nano Letters* **18**, 785 (2018).
- [36] J. Klicpera, J. Groß, and S. Günnemann, Directional message passing for molecular graphs, arXiv preprint arXiv:2003.03123 (2020).
- [37] S. Bernstein, Démonstration du théorème de Weierstrass fondée sur le calcul des probabilités, *Communications of the Kharkov Mathematical Society* **13**, 1 (1912).
- [38] N. Thomas, T. Smidt, S. Kearnes, L. Yang, L. Li, K. Kohlhoff, and P. Riley, Tensor field networks: Rotation-and translation-equivariant neural networks for 3d point clouds, arXiv preprint arXiv:1802.08219 (2018).
- [39] B. Anderson, T.-S. Hy, and R. Kondor, Cormorant: Covariant molecular neural networks, arXiv preprint arXiv:1906.04015 (2019).
- [40] K. T. Schütt, O. T. Unke, and M. Gastegger, Equivariant message passing for the prediction of tensorial properties and molecular spectra, arXiv preprint arXiv:2102.03150 (2021).
- [41] S. Batzner, T. E. Smidt, L. Sun, J. P. Mailoa, M. Kornbluth, N. Molinari, and B. Kozinsky, SE(3)-equivariant graph neural networks for data-efficient and accurate interatomic potentials, arXiv preprint arXiv:2101.03164 (2021).
- [42] A. P. Bartók, R. Kondor, and G. Csányi, On representing chemical environments, *Physical Review B* **87**, 184115 (2013).
- [43] A. P. Thompson, L. P. Swiler, C. R. Trott, S. M. Foiles, and G. J. Tucker, Spectral neighbor analysis method for automated generation of quantum-accurate interatomic potentials, *Journal of Computational Physics* **285**, 316 (2015).
- [44] N. Artrith, T. Morawietz, and J. Behler, High-dimensional neural-network potentials for multicomponent systems: Applications to zinc oxide, *Physical Review B* **83**, 153101 (2011).
- [45] T. Morawietz, V. Sharma, and J. Behler, A neural network potential-energy surface for the water dimer based on environment-dependent atomic energies and charges, *The Journal of Chemical Physics* **136**, 064103 (2012).
- [46] T. Morawietz and J. Behler, A density-functional theory-based neural network potential for water clusters includ-
- ing van der Waals corrections, *The Journal of Physical Chemistry A* **117**, 7356 (2013).
- [47] E. Uteva, R. S. Graham, R. D. Wilkinson, and R. J. Wheatley, Interpolation of intermolecular potentials using Gaussian processes, *The Journal of Chemical Physics* **147**, 161706 (2017).
- [48] K. Yao, J. E. Herr, D. W. Toth, R. Mckintyre, and J. Parkhill, The TensorMol-0.1 model chemistry: a neural network augmented with long-range physics, *Chemical science* **9**, 2261 (2018).
- [49] S. Grimme, J. Antony, S. Ehrlich, and H. Krieg, A consistent and accurate *ab initio* parametrization of density functional dispersion correction (DFT-D) for the 94 elements H-Pu, *The Journal of Chemical Physics* **132**, 154104 (2010).
- [50] E. Caldeweyher, S. Ehlert, A. Hansen, H. Neugebauer, S. Spicher, C. Bannwarth, and S. Grimme, A generally applicable atomic-charge dependent london dispersion correction, *The Journal of Chemical Physics* **150**, 154122 (2019).
- [51] J. F. Ziegler, U. Littmark, and J. P. Biersack, *The stopping and range of ions in solids* (Pergamon, New York, 1985).
- [52] S. A. Ghasemi, A. Hofstetter, S. Saha, and S. Goedecker, Interatomic potentials for ionic systems with density functional accuracy based on charge densities obtained by a neural network, *Physical Review B* **92**, 045131 (2015).
- [53] A. K. Rappe and W. A. Goddard III, Charge equilibration for molecular dynamics simulations, *The Journal of Physical Chemistry* **95**, 3358 (1991).
- [54] C. E. Wilmer, K. C. Kim, and R. Q. Snurr, An extended charge equilibration method, *The Journal of Physical Chemistry Letters* **3**, 2506 (2012).
- [55] Y.-T. Cheng, T.-R. Shan, T. Liang, R. K. Behera, S. R. Phillpot, and S. B. Sinnott, A charge optimized many-body (comb) potential for titanium and titania, *Journal of Physics: Condensed Matter* **26**, 315007 (2014).
- [56] T. W. Ko, J. A. Finkler, S. Goedecker, and J. Behler, A fourth-generation high-dimensional neural network potential with accurate electrostatics including non-local charge transfer, *Nature Communications* **12**, 398 (2021).
- [57] A. Griewank, On automatic differentiation, *Mathematical Programming: Recent developments and applications* **6**, 83 (1989).
- [58] D. Hendrycks and K. Gimpel, Gaussian error linear units (GELUs), arXiv preprint arXiv:1606.08415 (2016).
- [59] S. Elfwing, E. Uchibe, and K. Doya, Sigmoid-weighted linear units for neural network function approximation in reinforcement learning, *Neural Networks* **107**, 3 (2018).
- [60] P. Ramachandran, B. Zoph, and Q. V. Le, Searching for activation functions, arXiv preprint arXiv:1710.05941 (2017).
- [61] V. Nair and G. E. Hinton, Rectified linear units improve restricted boltzmann machines, in *ICML* (2010).
- [62] G. Cybenko, Approximation by superposition of sigmoidal functions, *Mathematics of Control, Signals, and Systems* **2**, 303 (1989).
- [63] K. Hornik, Approximation capabilities of multilayer feed-forward networks, *Neural Networks* **4**, 251 (1991).
- [64] R. Eldan and O. Shamir, The power of depth for feedforward neural networks, in *Conference on Learning Theory* (2016) pp. 907–940.

- [65] N. Cohen, O. Sharir, and A. Shashua, On the expressive power of deep learning: A tensor analysis, in *Conference On Learning Theory* (2016) pp. 698–728.
- [66] M. Telgarsky, Benefits of depth in neural networks, in *Conference On Learning Theory* (2016) pp. 1517–1539.
- [67] Z. Lu, H. Pu, F. Wang, Z. Hu, and L. Wang, The expressive power of neural networks: A view from the width, *Advances in Neural Information Processing Systems* **30**, 6231 (2017).
- [68] X. Glorot and Y. Bengio, Understanding the difficulty of training deep feedforward neural networks, in *Proceedings of the thirteenth international conference on artificial intelligence and statistics* (JMLR Workshop and Conference Proceedings, 2010) pp. 249–256.
- [69] R. K. Srivastava, K. Greff, and J. Schmidhuber, Highway networks, arXiv preprint arXiv:1505.00387 (2015).
- [70] K. He, X. Zhang, S. Ren, and J. Sun, Deep residual learning for image recognition, in *Proceedings of the IEEE conference on computer vision and pattern recognition* (2016) pp. 770–778.
- [71] K. He, X. Zhang, S. Ren, and J. Sun, Identity mappings in deep residual networks, in *European conference on computer vision* (Springer, 2016) pp. 630–645.
- [72] A. Vaswani, N. Shazeer, N. Parmar, J. Uszkoreit, L. Jones, A. N. Gomez, L. Kaiser, and I. Polosukhin, Attention is all you need, arXiv preprint arXiv:1706.03762 (2017).
- [73] J. Hoja, L. M. Sandonas, B. G. Ernst, A. Vazquez-Mayagoitia, R. A. DiStasio Jr, and A. Tkatchenko, QM7-X, a comprehensive dataset of quantum-mechanical properties spanning the chemical space of small organic molecules, *Scientific Data* **8**, 43 (2021).
- [74] J. Hermann, Z. Schätzle, and F. Noé, Deep-neural-network solution of the electronic Schrödinger equation, *Nature Chemistry* , 1 (2020).
- [75] G. J. Kowalski, *Information retrieval systems: theory and implementation*, Vol. 1 (Springer, 2007).
- [76] K. Choromanski, V. Likhoshesterov, D. Dohan, X. Song, A. Gane, T. Sarlos, P. Hawkins, J. Davis, A. Mohiuddin, L. Kaiser, D. Belanger, L. Colwell, and A. Weller, Rethinking attention with performers, arXiv preprint arXiv:2009.14794 (2020).
- [77] M. Gastegger, J. Behler, and P. Marquetand, Machine learning molecular dynamics for the simulation of infrared spectra, *Chemical Science* **8**, 6924 (2017).
- [78] A. Tkatchenko and M. Scheffler, Accurate molecular van der Waals interactions from ground-state electron density and free-atom reference data, *Physical Review Letters* **102**, 073005 (2009).
- [79] A. Tkatchenko, R. A. DiStasio Jr, R. Car, and M. Scheffler, Accurate and efficient method for many-body van der Waals interactions, *Physical Review Letters* **108**, 236402 (2012).
- [80] J. Hermann, R. A. DiStasio Jr, and A. Tkatchenko, First-principles models for van der Waals interactions in molecules and materials: Concepts, theory, and applications, *Chemical Reviews* **117**, 4714 (2017).
- [81] S. N. Pozdnyakov, M. J. Willatt, A. P. Bartók, C. Ortner, G. Csányi, and M. Ceriotti, Incompleteness of atomic structure representations, *Physical Review Letters* **125**, 166001 (2020).
- [82] A. Glielmo, C. Zeni, and A. De Vita, Efficient non-parametric n -body force fields from machine learning, *Physical Review B* **97**, 184307 (2018).
- [83] O. A. Von Lilienfeld, R. Ramakrishnan, M. Rupp, and A. Knoll, Fourier series of atomic radial distribution functions: A molecular fingerprint for machine learning models of quantum chemical properties, *International Journal of Quantum Chemistry* **115**, 1084 (2015).
- [84] E. Kocer, J. K. Mason, and H. Erturk, Continuous and optimally complete description of chemical environments using spherical Bessel descriptors, *AIP Advances* **10**, 015021 (2020).
- [85] F. A. Faber, A. S. Christensen, B. Huang, and O. A. Von Lilienfeld, Alchemical and structural distribution based representation for universal quantum machine learning, *The Journal of Chemical Physics* **148**, 241717 (2018).
- [86] S. Pozdnyakov, M. Willatt, and M. Ceriotti, Randomly-displaced methane configurations, Materials Cloud Archive 2020.110 (2020), <https://doi.org/10.24435/materialscloud:qy-dp>.
- [87] J. P. Perdew, K. Burke, and M. Ernzerhof, Generalized gradient approximation made simple, *Physical Review Letters* **77**, 3865 (1996).
- [88] L. C. Blum and J.-L. Reymond, 970 million druglike small molecules for virtual screening in the chemical universe database GDB-13, *Journal of the American Chemical Society* **131**, 8732 (2009).
- [89] C. Adamo and V. Barone, Toward reliable density functional methods without adjustable parameters: The PBE0 model, *The Journal of Chemical Physics* **110**, 6158 (1999).
- [90] T. W. Ko, J. A. Finkler, S. Goedecker, and J. Behler, A fourth-generation high-dimensional neural network potential with accurate electrostatics including non-local charge transfer, Materials Cloud Archive 2020.137 (2020), <https://doi.org/10.24435/materialscloud:f3-yh>.
- [91] F. L. Hirshfeld, Bonded-atom fragments for describing molecular charge densities, *Theoretica Chimica Acta* **44**, 129 (1977).
- [92] P. P. Ewald, Die Berechnung optischer und elektrostatischer Gitterpotentiale, *Annalen der Physik* **369**, 253 (1921).
- [93] M. Schwick, D. N. Tahchieva, and O. A. von Lilienfeld, The QMspin data set: Several thousand carbene singlet and triplet state structures and vertical spin gaps computed at MRCISD+Q-F12/cc-pVDZ-F12 level of theory, Materials Cloud Archive 2020.0051/v1 (2020), <https://doi.org/10.24435/materialscloud:2020.0051/v1>.
- [94] M. Schwick, D. N. Tahchieva, and O. A. von Lilienfeld, Large yet bounded: Spin gap ranges in carbenes, arXiv preprint arXiv:2004.10600 (2020).
- [95] S. J. Reddi, S. Kale, and S. Kumar, On the convergence of Adam and beyond, arXiv preprint arXiv:1904.09237 (2019).
- [96] C. Bannwarth, S. Ehlert, and S. Grimme, GFN2-xTB – an accurate and broadly parametrized self-consistent tight-binding quantum chemical method with multipole electrostatics and density-dependent dispersion contributions, *Journal of Chemical Theory and Computation* **15**, 1652 (2019).
- [97] K. Schütt, P. Kessel, M. Gastegger, K. Nicoli, A. Tkatchenko, and K.-R. Müller, Schnetpack: A deep learning toolbox for atomistic systems, *Journal of Chemical Theory and Computation* **15**, 448 (2018).
- [98] A. S. Christensen, F. A. Faber, B. Huang, L. A. Bratholm, A. Tkatchenko, K. R. Müller, and O. A. von

- Lilienfeld, QML: A python toolkit for quantum machine learning, <https://www.qmlcode.org> (2017).
- [99] T. Darden, D. York, and L. Pedersen, Particle mesh ewald: An $N \cdot \log(N)$ method for Ewald sums in large systems, *The Journal of Chemical Physics* **98**, 10089 (1993).
- [100] C. J. Fennell and J. D. Gezelter, Is the Ewald summation still necessary? pairwise alternatives to the accepted standard for long-range electrostatics, *The Journal of Chemical Physics* **124**, 234104 (2006).
- [101] A. Paszke, S. Gross, F. Massa, A. Lerer, J. Bradbury, G. Chanan, T. Killeen, Z. Lin, N. Gimelshein, L. Antiga, *et al.*, PyTorch: An imperative style, high-performance deep learning library, arXiv preprint arXiv:1912.01703 (2019).
- [102] J. Hoja, L. M. Sandonas, B. Ernst, A. Vazquez-Mayagoitia, R. A. J. DiStasio, and A. Tkatchenko, QM7-X: A comprehensive dataset of quantum-mechanical properties spanning the chemical space of small organic molecules, (Version 1.0) [Data set] Zenodo (2020), <http://doi.org/10.5281/zenodo.3905361>.